Trabajo de Fin de Grado
Facultad de ciencas
Sección de Física

A pilot study to test the reliability of O II model atoms with stellar spectroscopy

Author:
José Andrés Avellaneda González

Advisors:
Dr. Sergio Simón-Díaz
Dr. Yeisson Osorio

Curso 2020-2021

Contents

1 Resumen

La espectroscopía cuantitativa puede ser definida como la disciplina que permite inferir parámetros físicos a partir de la aplicación de herramientas de análisis espectroscópico a un espectro observado. Actualmente existe una gran cantidad de espectros de alta calidad que permiten el estudio detallado de las propiedades físicas de las estrellas en distintas ventanas espectrales. Para el estudio de las estrellas el espectro observado no es la única herramienta necesaria, el análisis cuantitativo requiere de un marco teórico sobre el cual comparar las observaciones e inferir parámetros físicos. En la astrofísica moderna este marco teórico es conocido como transporte radiativo y se materializa de manera práctica mediante los denominados **modelos de atmósfera**.

Los modelos de atmósfera permiten resolver el problema del transporte radiativo en la estrella con el objetivo de crear un **espectro estelar sintético**. *Es decir, permiten deducir la forma del espectro que emana del estrella y es medido por nuestros telescopios. Además de consideraciones con respecto a ciertos aspectos macroscópicos de la estrella (referentes tanto a la geometría considerada en el modelado como a los parámetros físicos fundamentales que caracterizan a la misma). Los modélos de atmósfera necesitan módelos atómicos fiables para representar la interacción radiación-materia que sucede en la estrella. El objetivo de este trabajo es el de testear dos módelos atómicos de O* II *construidos con el paquete computacional maKe Atoms Simple (KAS) desarrollado por Yeisson Osorio. Las comparación se realizará a través del cálculo de la abundancia de oxígeno en la estrella BD+463474 usando el método de la curva de crecimiento. Las observaciones (cuyo análisis espectroscópico fue ya presentado en García-Rojas et al., 2014) fueron realizadas con el espectrógrafo de alta resolución FIES montado en el telescopio NOT en el observatorio del Roque de los Muchachos el 10 de septiembre de 2012. Esta estrella, ubicada en la nebulosa del Capullo, es una buena candidata para el testeo de modelos atómicos debido a su baja rotación y parámetros estelares favorables.*

Con el objetivo de comparar los modelos atómicos, dos redes de espectros sintéticos (en los que, fijadas la temperatura efectiva y la gravedad superficial de la estrella, se dejaron variar la abundancia de oxígeno y la microturbulencia) fueron calculados. Para el cáculo de los espectros se utilizó el programa de cálculo de atmósferas estelares llamado TLUSTY, el cual fue alimentado con cada modelo atómico para el cálculo de cada respectiva red. En este sentido en la sección 4 se da un pequeño acercamiento a la construcción de modelos atómicos. Así mismo, en esta sección se realizará una revisión detallada de las principales diferencias entre los dos modelos atómicos utilizados en nuestro estudio. Cabe destacar, también, que uno de los objetivos de este trabajo fue desarrollar un paquete computacional en IDL con la finalidad de compatibilizar la salida del programa de cálculo de espectros sintéticos con un programa de cálculo de abundancias desarrollado por Sergio Simón-Díaz.

Este trabajo se inició con la selección de una lista preliminar de 46 líneas de absorción de O II. *Para la selección se partió de una lista de líneas proporcionada por el sistema KAS. De donde se fueron descartando líneas por motivos de contaminación, blending, dificultad para medir su anchura equivalente o problemas en el espectro sintético hasta llegar a la lista preliminar de 46 líneas de O* II. *La metodología utilizada para la selección y cálculo de contaminación de las líneas se detalla en la sección 5. En esta sección se desarrolla también el método de la curva de crecimiento y el efecto que tienen los distintos parámetros estelares en el resultado del cálculo de abundancias.*

Nuestros análisis arrojaron que los modelos utilizados dan resultados en concordancia con los derivados por García-Rojas et al. (2014). Luego de comprobar que los modelos pueden, de manera global, llevar un análisis completo de abundancias procedimos a analizar el set de líneas dividido por multipletes. Este acercamiento nos permitió analizar la sensibilidad de cada multiplete con respecto a cambios en el módelo atómico, así como también descubrir problemas en la información atómica usada para calcular los espectros sintéticos. El estudio por multipletes logró demostrar principalmente que: el grado de sensibilidad con respecto a cambios en el modelo atómico depende del multiplete, las líneas más fuertes parecen demostrar mayor sensibilidad que las más debiles, existen deficiencias en algunos valores de la información atómica considerada y que la sensibilidad a cambios en los modelos parece ser menor a microturbulencias mayores. Por último nuestros análisis permitieron desarrollar una metodología que puede ser aplicable para otras estrellas de parámetros estelares similares con otras especies químicas y con un número mayor de modelos atómicos. En

la sección 6 damos una revisión profunda de los resultados más importantes de nuestro análisis. Mientras que, en la sección 7, se desarrollan las conclusiones finales y los futuros curso de acción a tomar partiendo de la metodología desarrollada.

2 Introduction

Esta sección presenta una pequeña introducción a la espectroscopía cuantitativa y al concepto de atmósferas estelares y modelos atómicos. Se hace un también enfásis en la importancia del estudio del espectro estelar y, en específico, del tipo de estrella que se utiliza en este trabajo.

Since the first developments of modern spectroscopy in the nineteenth century, most notably by Joseph Von Fraunhofer (Jackson, 2000), spectroscopy has become a crucial tool for astronomers in their constant attempt to test their theories and gain insight into the components of astronomical objects. The astronomers of today are not an exception. Most of current observational astronomy is based on spectroscopic tools, thanls to the large amount of high quality data being collected regularly with modern telescope facilities. Stellar spectroscopy, the basis of this work, refers to the study of the spectra of stars in order to obtain information regarding their physical properties and (surface) chemical composition. The high resolution stellar spectra now available allows for a detailed line absorption analysis in a wide range of wavelengths.

Stellar spectroscopy can be considered of utmost importance in modern astrophysics. Not only to gain information about starts themselves but also thanks to the the hints it gives us about the evolution of galaxies and the universe itself. A star carries within information concerning several important aspects of astrophysics and that information is made available to researchers mostly through its spectra. The energy generated in the stellar interior escapes from the star in the form of radiation (light) through the so-called stellar atmosphere. A part of the star that can be thought of as the zone transitioning between the stellar interior and the interstellar medium (Gray, 2008). However, most of the visible stellar spectrum comes from a thin part called the photosphere. When light passes trough the photosphere it interacts with the chemical species which absorb some of the energy at specific wavelengths. Then, the spectrum emanating from the photosphere carries an imprint of its physical properties (e.g. Temperature and density) and chemical composition. Having this in mind quantitative spectroscopy could be defined as the discipline of inferring physical parameters of a star by applying spectroscopic tools to an observed spectrum (Simón-Díaz, 2020).

For this work we will center in the massive OB star spectral types, which can be considered to be an spectroscopic 'natural group' in which, at intermediate and high spectral resolution Helium absorption line detection is possible (Simón-Díaz, 2020). It is characteristic of these stars to have their spectra populated with large numbers of O II lines along with other H I, He I-II and Si II-IV lines. The study of OB stars proves to be specially useful when investigating present day abundance patterns in the the Milky Way and other galaxies. It is with this goal in mind that oxygen appears to be an element on which researchers should lie a careful eye. The study of oxygen could lead researchers into results with the potential of changing our perspective on stellar formation or chemo-dynamical evolution of galaxies (Stasinska et al., 2012). Moreover, being the most abundant of the metals and having well understood formation processes oxygen abundance analysis presents itself to be more feasible than similar studies on other elements.

Apart from an observational spectrum, an abundance analysis requires a theoretical framework in order to compare the observations and infer physical parameters. In stellar astrophysics these basis are known as 'model atmospheres'. As the formation of stellar spectra is a complicated process involving many physical variables there is no way to make direct deductive predictions on the matter. Instead a *stellar model atmosphere* is constructed by considering a series of simplifying assumptions with the goal of being able to produce a synthetic spectrum from a set of stellar parameters and a given chemical composition. The main assumptions current standard model atmospheres rely on are:

- One dimensional geometry (1D): Plane-parallel or spherical symmetry in the star's atmosphere is assumed. The stellar atmosphere is then described by layers stacked radially. For dwarf and not too extreme giant stars the plane-parallel geometry approximation is used.
- Time independence. Static conditions or constant flow speeds are assumed in order to simplify the momentum equation.
- Chemical homogeneity. The relative mixture of chemical elements are assumed to be the same everywhere

- Absence of magnetic fields.

In hot starts line blanketing effects and non-local thermodynamic equilibrium (NLTE) must be considered as well. Apart from the stellar parameters, the stellar atmospheres codes need reliable atomic data to perform their calculations. Feeding inaccurate atomic data to the code will only results in an erroneous construction of the synthetic spectrum and, in turn, force the abundance analysis to give spurious results. Roughly speaking building a model atom requires the definition of the energy levels and a whole set of continuum and line processes, both collisional and radiative (Przybilla, 2010). The high precision and sophistication reached by stellar models make the correct construction of atomic models a current concern in stellar astrophysics. Once the synthetic spectrum is calculated the approach is to compare the observed spectrum with a grid of synthetic ones until the agreement with the observations is reached (or, at least, maximized).

3 Objectives

Los objetivos de nuestro estudio son presentados en esta sección. En primer lugar se presenta el paquete computacional utilizado para el cálculo de los modelos atómicos junto con el modelo de atmósfera escogido. Se menciona, también, que la metodología seguida para el cálculo de abundancias corresponde con el método de la curva de crecimiento. Por último se hace un pequeño resumen de la estructura del trabajo.

The purpose of our study is to test two different model atoms, constructed with the *maKe Atoms Simple (KAS)* computational package developed by Yeisson Osorio (Osorio, 2018). This will be done by means of the curve of growth method, where the equivalent width of a given line is related to the chemical element abundance (see a detailed explanation in section 5.3.1). Using this method we will calculate the abundance of oxygen in the B0.5 V star BD+463474 with both of our model atoms and compare the results. The ultimate objective is to look for discrepancies between the two versions of the O II model atom in order to check their reliability, test the sensitivity of absorption lines to changes in model atoms and find potential errors in the basic atomic data considered for the synthetic spectrum calculation. For this reason two complete grids of synthetic spectra, dependent on a series of stellar parameters (in which effective temperature and surface gravity are kept fixed while abundance and microturbulence are left as free parameters), will be computed by feeding each model atom to the plane-parallel, line-blanketed, non-LTE stellar atmosphere code TLUSTY (Hubeny, 1988) and its associated spectrum synthesis code SYNSPEC.

Special care will be put into finding the best set of absorption lines available in the comprehensive line list provided also by the KAS system and securing their adequacy to the specific physical conditions of the star under study. Moreover, extensive study will also be made on the potential contamination of the preliminary set of lines chosen. Particular attention will also be put into securing that the same methodology could be used to study other stars of the same spectral types.

This work will follow a self consistent approach. In the first place, the tools needed to perform a quantitative spectroscopic analysis are presented in section 4. Special attention will be given to a thorough review on the calculation of model atoms and the the description of the main differences characterizing the two version of the O II model atoms considered in this work. Next, we present (in Sect. 5) the main steps defining the analysis strategy followed in this study, from the identification of diagnostic lines to the determination of the oxygen abundance. In addition, this section will contain a brief review of the stellar parameter's effect on absorption lines in the context of the curve of growth method. Finally, detailed analysis of the results and the presentation of our final conclusions is given in section 6 and 7 respectively.

4 Tools

Esta sección esta dedicada a una presentación de las tres herramientas que se necesitarán para completar el estudio. El espectro observado, los modelos atómicos y los espectros sintéticos. En primer lugar se comenta sobre el espectro de la estrella selecionada para este trabajo (BD +463474), y el porqué de su utilidad para nuestros objetivos. Luego, se da un pequeño resumen de la consideraciones más importantes a la hora de la construcción de un modelo atómico, para terminar en una explicación detallada de las diferencias entre nuestros dos modelos. Por último se explica brevemente el proceso de construcción del espectro sintético junto con los parámetros estelares considerados para la construcción de las redes.

In addition to a model atmosphere, which was selected to be calculated using TLUSTY, any quantitative spectroscopic analysis is based in an specific set of tools. In this section we will present and review the three main ingredients considered in this work: The observed spectrum, the model atoms and the synthetic spectra.

4.1 Targeted star and observed spectrum

BD+463474 is a B0.5 V type star located at the center of the Coccon nebula, in the constellation of Cygnus. Its low projected rotational velocity along with its stellar parameters make this star a perfect candidate to be used for the main purpose of this work: testing two different versions of the OII model atom using stellar spectroscopy. The spectroscopic observations of the BD+463474 star were carried out with the FIES cross-dispersed, high resolution echelle spectrograph attached to the 2.56m NOT telescope at El Roque de los Muchachos observatory on 2012 September 10. Using this observational spectrum García-rojas et al. (2014) performed a complete quantitative spectroscopic analysis of the star in order to derive its physical parameters (and oxygen abundance), which are summarized in Table 1.

$T_{\rm eff}$(K)	30500±1000
log g (dex)	4.2±0.1
ξ_t(km s^{-1})	<5
$v$sin$i$	<15
log(O/H)+12	8.73±0.08

Table 1: *Derived stellar parameters for the star BD+463474 (see García-Rojas et al. 2014). For completeness and to compare with the results of this work we also include the oxygen abundance derived by these authors.*

4.2 Model Atoms

The necessity of finding, in terms of stellar astrophysics, the best possible representation of the behaviour of ions in the stellar atmospheres rests in the key role it plays in the computation of synthetic spectra. As mentioned before, model atmosphere codes need reliable model atoms fed into them in order to complete the calculation of synthetic spectra. On that account, this section is dedicated to a review of the basic considerations that must be taken into account for the calculation of atomic level populations in stellar plasma and a presentation of the differences between the two model atoms compared in this study.

4.2.1 LTE and NLTE

A stellar atmosphere in thermodynamic equilibrium can be understood as one that has its momentum, particle internal degrees of freedom and internal degrees of freedom of the electromagnetic field distributions fixed to their equilibrium values (Kubát, 2014). In addition, by definition,

a system in thermodynamic equilibrium experience no change when isolated. In thermodynamic equilibrium the radiation field follows a Planck distribution and the velocity field a Maxwell distribution. Moreover, level populations follow the Boltzmann distribution (Eq. 1) for levels within an ion .

$$\frac{n_{i,j}}{n_{l,j}} = \frac{g_{i,j}}{g_{l,j}} e^{-(E_l - E_i)/kT} \tag{1}$$

where $n_{i,j}$ is the equilibrium population and $g_{i,j}$ the statistical weight of the level i of ion j and E_i is the energy of level i. And the Saha equation for levels between ions.

$$\frac{n_{i+1} n_e}{n_i} = \frac{2}{\lambda^3} \frac{g_{i+1}}{g_i} e^{-\chi_{0i}/k_b T} \tag{2}$$

where n_i is the density of atoms in the i-th state of ionization, g_i is the degeneracy of states for the i-ions, n_e is the electron density, λ is the thermal De Broglie wavelength of an electron and χ_{oi} the excitation energy of the i-ion. Nevertheless, stellar atmospheres cannot be described by full thermodynamic equilibrium. In order for the radiation to be able to escape from the stellar atmosphere there must be some degree of depth dependent density and temperature in the star, breaking the thermodynamic equilibrium. Hence, with the goal of preserving the simplicity of the considerations of thermodynamic equilibrium the notion of *Local thermodynamic equilibrium (LTE)* is introduced, allowing the (local) use of the Maxwell and Boltzmann equilibrium distributions with the consideration of a local temperature T and electron density n_e. The difference between LTE and full thermodynamic equilibrium lies in the fact that the radiation field is no longer in equilibrium and thus has to be calculated by solving the radiative transfer equation.

Depending on the balance between radiation and collisional processes the distribution of level populations could deviate from the Saha/Boltzmann distribution. Should the deviation occur the system is said to be in *Non-Local thermodynamic equilibrium (NLTE)*. In both LTE and NLTE the velocity distribution is taken to be Maxwellian, elastic collisions between particles preserve the equilibrium distribution; hence, it is the inelastic collisions that drive the system out of LTE. In that sense, radiation processes also cause the system to fall out of LTE, making NLTE a more accurate consideration. In practice, the basic difference between LTE and NLTE is the way in which atomic level populations are calculated (See Sect. 4.2.5 for a summary of level population calculation in NLTE).

4.2.2 Radiative Transport

Radiation is the primary form of energy transport through the surface layers of a star (Gray, 2008). Now, as it is the interaction between the radiation field and chemical species in the photosphere one of the mechanisms giving rise to the observed spectra, the problem of radiative transport is one that concerns almost all fields of stellar astrophysics. In the realm of model atom construction, to be specific, radiative excitation is one of the two main mechanisms governing the level populations and so, for an accurate model to be calculated, the light emanating form the inner layers of the star must be understood. The radiative transfer problem must be solved.

First let's introduce the concept of specific intensity. Which, at a point on a surface, at a given time, at the direction θ, at frequency ν, could be defined by:

$$I_\nu = lim \frac{\Delta E_\nu}{cos\theta \Delta A \Delta\omega \Delta t \Delta\nu} \tag{3}$$

where ΔA is a small portion of surface, $\Delta\nu$ the increment in spectral band, $\Delta\omega$ the increment of solid angle, Δt the increment in time and ΔE_ν the increment in energy at a frequency ν. Then, if

we consider radiation travelling in a direction s the change in specific intensity over an increment of path length ds can be attributed to the simple sums of the losses and gains, given by equation:

$$dI_\nu = -\kappa_\nu \rho I_v ds + j_v \rho ds \tag{4}$$

with j_ν and κ_ν being the emission and absorption coefficients. If we now divide the equation by $\kappa_\nu \rho ds$, defined as increment of optical depth, we get the equation of radiative transfer

$$\frac{dI_v}{d\tau_v} = -I_v + \frac{j_v}{\kappa_v} \tag{5}$$

Solving this equation enable us to find the mean intensity, defined as the directional average of the specific intensity which is needed for the determination of level populations (Przybilla, 2010).

$$J_v = \frac{1}{4\pi} \oint I_v d\omega \tag{6}$$

4.2.3 Radiative Transitions

Atomic physics states that electrons in the atom are in bound states with an specific energy. Any electron transition between those states results in an emission/absorption of a photon with frequency proportional to the difference in energy of the levels according to Planck's relation, an spectral line. Transitions of this type are called *bound-bound transitions* since they happen between bound states. Also, as incoming radiation comes in a continuum of wavelengths, there are photons that reach the photosphere with enough energy to ionize the atom, freeing the electron; these types of interactions are called *bound-free transitions*. In the case of spectral lines their strength is directly determined by the number of absorbers (abundance) and the line absorption cross section (Przybilla, 2010), given by

$$\sigma_{ij} = \frac{\pi e^2}{m_e c} f_{ij} \phi(\nu) \tag{7}$$

Where $\phi(\nu)$ is the line absorption profile (which can be approximated by a Doppler profile in most cases, m_e the mass of the electron and e the electron charge. f_{ij} is the oscillator strength, a dimensionless response function, in the first place applied to electric dipole transitions (Nahar, 2011). It is a measure of the strength of an atomic transition and the intensity of a spectral line. It is in the selection of the right set of oscillator strengths that one of the problems of model atom construction resides, there is no definitive answer to what set of data should be used in general. It is to be noted that the oscillator strengths usually refers to the *absorption* strength; which is related to the *emission* strength via detailed balance.

$$f_{ij} = \frac{g_j}{g_i} f_{ji} \quad (\text{or as } \prime gf - \text{values}\prime \;\; g_i f_{ij} = g_j f_{ji}) \tag{8}$$

Radiative transitions are constricted by *selection rules* limiting the states between which a transition has a non-negligible probability of occurring. Transitions between bound states limited by selection rules are called *Forbidden Transitions*. The inclusion of this kind of transitions is possible during the calculation of model atoms and it comprises one of the key differences between the two models used in this study. More on the specifics of the model atoms used in this work is given in upcoming sections.

4.2.4 Collisional Transitions

The energy coming from the inner layers of the star is also transferred to its constituent particles in the form of kinetic energy. The velocity distribution assumed is generally Maxwellian, given by

the local plasma temperature (Przybilla, 2010). Inside the ionized plasma inelastic collisions may also cause excitation (or even ionization) of the ions present. In general, only electron collisions are to be considered due to their high thermal velocity in comparison with heavy particles.

Unlike radiative transitions, collisional transitions are not restricted by selection rules and therefore serve as the primary mechanisms for exciting low lying transitions with levels of the same parity (Nahar, 2011). Collisional ionization, on the other hand, helps to determine the *ionization balance*, the relative distribution of ions of a given element in the plasma.

Inelastic cross sections for electron-ion scattering in units of the hydrogen atom cross section in the first Bohr radius are given by equation (Nahar, 2011),

$$Q_{ij} = \frac{\Omega_{ij}}{g_{ij}k_i^2}(\pi a_0^2) \tag{9}$$

Where Ω_{ij} is the collision strength (the equivalent of oscillator strength in radiative processes), g_i is the statistical weight of the initial level and $E = k_i^2$ is the energy of the incident electron in Rydbergs. For practical applications the average of the cross section over the velocity distribution $< vQ(v) >$ is preferred. However, Computationally speaking it is more convenient to use the Maxwellian averaged collision strength, given by

$$\Upsilon_{ij} = \int_0^\infty \Omega_{ij} e^{-E_j/kT} d(E_j/kT) \tag{10}$$

Where T is the temperature characterizing the Maxwellian velocity distribution.

4.2.5 Level Populations

The calculation of accurate occupation numbers is one of the key tasks to be completed in order for the model atom to be useful for comparison with observed spectral lines. In a steady state, the population of each level remain constant in time. hence, the general approach is to calculate the sum of all the incoming and outgoing rates and impose the steady state condition (Przybilla, 2010). Therefore, the equations to be solved (in NLTE) are those of the rate equations of statistical equilibrium, given by

$$\sum_{j\neq i} n_i(R_{ij} + C_{ij}) = \sum_{j\neq i} n_j(R_{ji} + C_{ji}) \tag{11}$$

where R_{ij} and C_{ij} are the radiative and collisional rates respectively, for transitions from level i and level j. Radiative rate is defined as

$$R_{ij} = 4\pi \int \sigma_{ij}(\nu)\frac{J_\nu}{h\nu} d\nu \tag{12}$$

where $\sigma_{ij}(\nu)$ is the radiative atomic cross section. Collisional upward rates, on the other hand, are given by

$$C_{ij} = n_e \int \sigma_{ij}(v) f(v) v dv \tag{13}$$

in this case $\sigma_{ij}(v)$ is the collisional cross section, n_e the electron density, v the velocity and $f(v)$ the, in general, Maxwellian distribution of the particles.

4.2.6 KAS Models

The two model atoms used in this study were constructed using the maKe Atoms Simple (KAS) Package developed in IDL by Yeisson Osorio. KAS is a computational package whose main purpose is the unification and comparison of atomic data from different sources in order to solve the radiative transfer equation in NLTE (Osorio, 2018). The atomic data needed for the models used in this study was collected from two different sources, the Atomic spectral database from the National institute of standards and technology [1] and the opacity project [2].

The difference between the two models lies in the energy levels and the bound-bound transitions used. TOP-BASE carries a quantum mechanical calculation of the energy levels and the allowed radiative transitions. In that way **Model 1** (TOP-BASE) is completely self-consistent. On the other hand, **Model 2** takes model 1 as a starting point but updates the energy levels with the experimental values coming from NIST. Bound-bound transitions existing both NIST and TOP-BASE are update while transitions that exist in NIST but not in TOP-BASE are added in model 2. Therefore, given that NIST includes the forbidden transitions these are included in model 2 as well. More information regarding the characteristics of the two models is summarized in Table 2. Furthermore, Fig. 1 shows the grotrian diagrams displaying the transition included in each model atom.

	Model 1	Model 2
Number of energy levels	220	303
Number of bound-bound transitions	3546	3660
Number of bound-free transitions	173	173

Table 2: Main differences between the two versions of tho O II used in this study. This table shows how Model 2 exhibits a greater number of energy levels and bound-bound transitions but the same number of bound-free transitions.

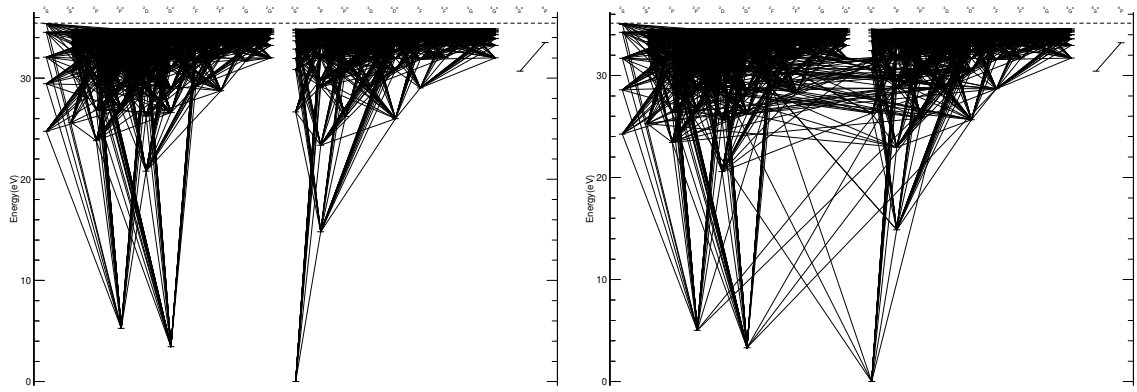

(a) *Model 1* **(b)** *Model 2*

Figure 1: Grotrian diagrams displaying the radiative transitions included in our O II model atoms

4.3 Synthetic spectra

A grid of synthetic spectra was calculated using the general spectrum synthesis program called *Synspec*. The program assumes an existing model atmosphere which, in our case, was calculated using TLUSTY. The stellar parameters used for the grid were chosen from existing TLUSTY model to be the closest available to those derived by García-Rojas et al. (2014). The grid values

[1] https://www.nist.gov/about-nist
[2] http://cdsweb.u-strasbg.fr/topbase/topbase.html

are presented below.

- Effecive Temperature: 30000K
- Surface Gravity: 4.25 dex
- Oxygen Abundances: [8.55, 8.65, 8.70, 8.75, 8.80, 8.85] dex
- Microturbulences: 1,3,5,7,9 km/s

5 Methodology

La sección de metodología está dedicada a una explicación detallada del proceso seguido para la identificación y el cálculo de contaminación de las líneas de O II. *Se explica también en este capítulo la metodología seguida para la medición de las anchuras equivalentes. Por último, se hace una revisión completa del cálculo de abundancias utilizando el método de la curva de crecimiento.*

The methodology followed in this study was first to find a suitable set of lines for the fixed stellar parameters, calculate their equivalent widths, use them to calculate their abundance through the curve of growth method and compare the results of the abundance analysis of our two model atoms. In this section the complete process of calculating the abundance of oxygen in this star, from the specifics of the curve of growth method, passing through the measurement of equivalent widths and finalizing in comments on the process of selection of the preliminary set of lines is explained.

5.1 Equivalent width measurement

The equivalent width of a spectral line in absorption (as is the case considered in this study) is defined as::

$$EW_\nu = \int \frac{F_c - F_\nu}{F_c} d\nu \tag{14}$$

Where F_c and F_ν are the continuum and line fluxes respectively. In the context of absorption lines F_ν denotes the energy transmitted from the continuum through absorption by an atomic transition at a frequency ν.

In this work, the measurement of equivalent widths of the O II diagnostic lines was carried using an IDL routine developed by Sergio Simón-Díaz and based on a least square profile fitting, with Gaussian profiles fitting the line and polynomials of degree one to fit the local continuum. As an input the procedure needs a spectrum, a list of line centers and the value of the radial velocity of the star with respect to the observer to make the Doppler correction. The program then returns a list naming every line with its respective equivalent width and error. Also, the program provides detailed snapshots of each considered diagnostic line, which serves to give additional information on the quality of the fitting. If the signal to noise ratio in that wavelength range is not good the fitting will be less reliable, a situation which can be identified in the snapshots. In order to keep consistency, the equivalent widths in both observed and synthetic spectra (see Sects. 4.1 and 4.3, respectively) will be measured using the same routine.

5.2 Line identification

The first task in this endeavour was to establish a set of suitable lines to be used. For line identification (and also all line contamination calculations) the comprehensive list of lines and synthetic spectra given by the KAS system was used, specifically the ones corresponding to model 1 with abundance 8.70 dex and microturbulence 5 km/s. This pair of values of abundance and microturbulence were deemed to best represent globally the suitability of lines as they are the center values in the calculated grid of synthetic spectra (Sect. 4.3). In this study we will focus exclusively on the range between 3900 and 7000 Å, the so-called optical range. We also decided to discard those lines with an equivalent width smaller than 15 mÅ due to its difficulty in being properly identified in the observed spectrum (due to the limited signal-to-noise ratio). Having applied these two constraints we obtained a tentative list of 189 O II lines. The next step then is to filter the remaining lines by their degree of contamination. A thorough explanation on the process carried to calculate the contamination of each line is given in the next section.

5.2.1 Line Contamination

Line blending is perhaps one the biggest problems when performing quantitative spectroscopic analysis based on measuring the equivalent widths. This section is dedicated to an explanation of the process of identification of potential blending effects in the tentative list of 189 O II lines. The outcome of the analysis presented in this section is summarized in the last column of Table 3.

The potential blending of a specific diagnostic line depends on the combination of two effects: (1) the separation between the line under study and other contaminating lines, and (2) the specific broadening of the lines. We must remark that the analysis must be performed for the specific conditions of each star. With that in mind, we note that the outcome of this exercise is only valid for the star under study. Other blends may occur for stars with different stellar parameters. Two broadening parameters were thus considered in this part. Rotational broadening and resolving power. In this work the resolution power was taken to be 85000 and $v\sin i$ twice the value derived by García-Rojas et al. (2014). We know that the resolution relation indicates that:

$$R = \frac{\lambda}{\Delta\lambda_{Resol}} \tag{15}$$

It is immediate to see that, as with Doppler broadening $\Delta\lambda$ increases linearly with λ. Rotational broadening, on the other hand, refers to the effect the rotation of the star has on the shape of absorption lines. As the star rotates different points of its surface have varying velocities with respect to the observer. Then, lines coming from different points will be affected be the Doppler effect differently. Points far from the center of the stellar disk being the ones where this effect is maximized. Rotational broadening does not affect the equivalent width of individual lines but may cause lines close enough to blend. We recall that the expression for rotational broadening states:

$$\frac{vsini}{c} = \frac{\Delta\lambda_{Rot}}{\lambda} \tag{16}$$

Since in this work we are mainly concentrating in metallic lines, we considered that two lines were blended if the wavelength separation ($\Delta\lambda$) was less or equal than:

$$\Delta\lambda = 2\sqrt{\Delta\lambda^2_{Resol} + \Delta\lambda^2_{Rot}} \tag{17}$$

Using this expression $\Delta\lambda$ was calculated for every one of the remaining 189 O II lines. Furthermore, taking advantage of the theoretical equivalent widths provided by the comprehensive line list we were able to calculate an approximate contamination percentage for every line used in this study. This percentage was found by comparing the sum of EWs of the contaminators to the EW of the O II line under consideration:

$$\%_{contamination} = \frac{\sum EW_{contaminators}}{EW_{O\ II}} \tag{18}$$

Results of calculations are shown in Fig. 2. As a first cleaning of the linelist, those lines with more than 50% contamination were discarded, leaving a preliminary total of 142 O II lines.

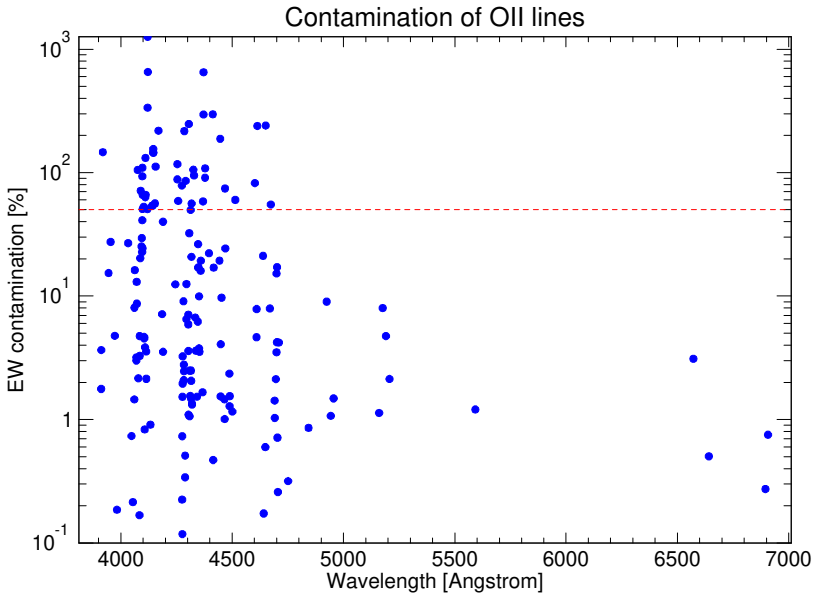

(a) *Logarithm of the contamination percentage for all of the remaining lines. Red dotted line marks contamination of 50%*

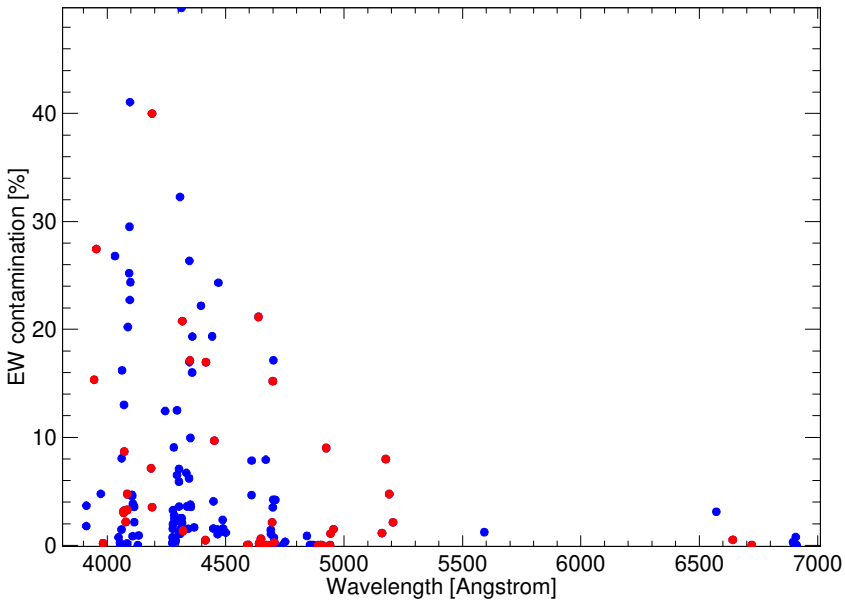

(b) *Linear plot of O* II *line contamination. Chosen lines (see Table 3) are plotted in red*

Figure 2: *PLots containing the results of our contamination analysis, each dot correspond to a O* II line coming from our list of lines

Not only this approach proved to be useful for finding the contaminators of O II lines but also to calculate which O II lines are sufficiently close between themselves to be considered blended. Furthermore, this quantitative study was completed with a careful qualitative analysis of the observed and synthetic spectra to search for any undetected problems with the remaining lines. This final analysis allowed us to reduce the tentative list from 142 to 46 O II absorption lines. Noting that the coming abundance analysis will most likely raise undetected issues with some lines that are yet to be noticed, the preliminary list of the remaining 46 O II lines is presented in Table 3. Atomic information was provided by the Atomic line list (Van Hoof, 2018) and by the line list used in the calculation of the synthetic spectra. In addition, Fig. 3 show the grotrian diagrams for

each model atom displaying the transitions corresponding to the multiplets summarized in Table 3.

Multiplet	Terms	Label	$\log(gf)_{SS}$	$\log(gf)_{ALL}$	λ_{SS}	λ_{ALL}	Notes
$2s^2.2p^2.(3P).3s\text{-}2s^2.2p^2.(3P).3p$							
1	$^4P\text{-}^4Do$	O II 4650	0.43	0.32	4649.14	4649.13	
		O II 4641	0.18	0.07	4641.83	4641.81	
		O II 4661	-0.17	-0.27	4661.64	4661.63	
		O II 4638	-0.26	-0.32	4638.86	4638.86	(+C II 4638.92 and C II 4639.07 21%)
		O II 4676	-0.30	-0.38	4676.24	4676.24	
		O II 4696	-0.98	-1.38	4696.36	4696.35	(+N II 4695.90 13%)
2	$^4P\text{-}^4P_o$	O II 4349	0.10	0.07	4349.43	4349.43	(+Fe II 4348.81 and Ne II 4349.13 17%)
		O II 4317	-0.33	-0.37	4317.15	4317.14	(+C II 4317.27 20%)
			-0.11	-	4317.78	4317.70	
		O II 4319	-0.32	-0.37	4319.64	4319.63	
			-0.47	-0.50	4319.88	4319.87	
3	$^2P\text{-}^2P_o$	O II 3954	-0.35	-0.40	3954.36	3954.36	(+Fe II 3953.76 and Fe II 3954.31/38 27%)
		O II 3982	-0.67	-0.69	3982.72	3982.71	
		O II 3945	-0.69	-0.71	3945.04	3945.04	(+C II 3945.00/23 15%)
4	$^2P\text{-}^2S_o$	O II 6721	-0.59	-0.63	6721.36	6721.40	
		O II 6641	-0.89	-0.90	6640.99	6641.03	
5	$^2P\text{-}^2D_o$	O II 4414	0.31	0.21	4414.88	4414.90	
			-3.50	-1.48	4414.59	4414.46	
		O II 4416	0.04	-0.04	4416.97	4416.97	(+Ne II 4416.76 and N II 4417.10/83 17%)
			-3.38	-	4416.62	4416.50	
		O II 4452	-0.74	-0.77	4452.38	4452.38	(+Ne II 4452.60 10%)
$2s^2.2p^2.(1D).3s\text{-}2s^2.2p^2.(1D).3p$							
6	$^2D\text{-}^2F_o$	O II 4590	0.45	0.33	4591.01	4590.97	
		O II 4596	0.29	0.18	4596.20	4596.18	
			-0.82	-1.02	4595.99	4595.96	
$2s^2.2p^2.(3P).3p\text{-}2s^2.2p^2.(3P).3d$							
7	$^4D_o\text{-}^4F$	O II 4072	0.53	0.53	4072.16	4072.15	(+Ar II 4072.00 2%)
		O II 4069	0.34	0.35	4069.89	4069.88	(+Fe II 4069.21 3%)
			0.14	0.14	4069.64	4069.62	
			-2.64	-4.42	4070.03	4070.06	
		O II 4086	-0.14	-0.19	4085.12	4085.11	(+Fe II 4084.83 3%)
			-0.89	-0.83	4084.65	4084.65	
		O II 4078	-1.46	-0.29	4078.86	4078.84	
8	$^2D_o\text{-}^2F$	O II 4705	0.57	0.53	4705.32	4705.35	
		O II 4699	0.41	0.24	4699.19	4699.22	(+Ne II 4698.43 and N II 4700.03 9%)
9	$^4S_o\text{-}^4P$	O II 4924	0.15	0.05	4924.52	4924.53	(+S II 4924.11 and S II 4925.34 9%)
		O II 4906	-0.03	-0.16	4906.82	4906.83	
		O II 4891	-0.33	-0.47	4890.85	4890.86	
$2s^2.2p^2.(3P).3p\text{-}2s^2.2p^2.(3P).3d$							
10	$^2P_o\text{-}^2D$	O II 4943	0.37	0.31	4943.00	4943.01	
		O II 4941	0.08	0.02	4941.10	4941.08	
		O II 4956	-0.42	-0.50	4955.74	4955.71	
$2s^2.2p^2.(3P).3p\text{-}2s^2.2p^2.(3P).3d$							
11	$^2P_o\text{-}^2P$	O II 5207	-0.86	-0.16	5206.71	5206.65	
		O II 5160	-0.66	-0.49	5160.03	5159.94	
		O II 5190	-0.55	-0.63	5190.56	5190.50	(+N II 5190.38 4%)
		O II 5175	-0.20	-0.80	5175.99	5175.90	(+N II 5175.89 8%
$2s^2.2p^2.(1D).3p\text{-}2s^2.2p^2.(1D).3d$							
12	$^2F_o\text{-}^2G$	O II 4189	0.83	0.72	4189.79	4189.79	
			-0.73	-0.83	4189.58	4189.58	(+S II 4189.68/59 and Fe II 4188.90 40%)
		O II 4185	0.71	0.60	4185.44	4185.44	(+Fe II 4184.98 4%)

Table 3: *Preliminary set of lines ordered by multiplets and energies. This table showcases the information coming from the Atomic line list (ALL) and the atomic data used in the calculation of the synthetic spectra (SS). Last column displays the results of the contamination analysis with calculated contamination percentage.*

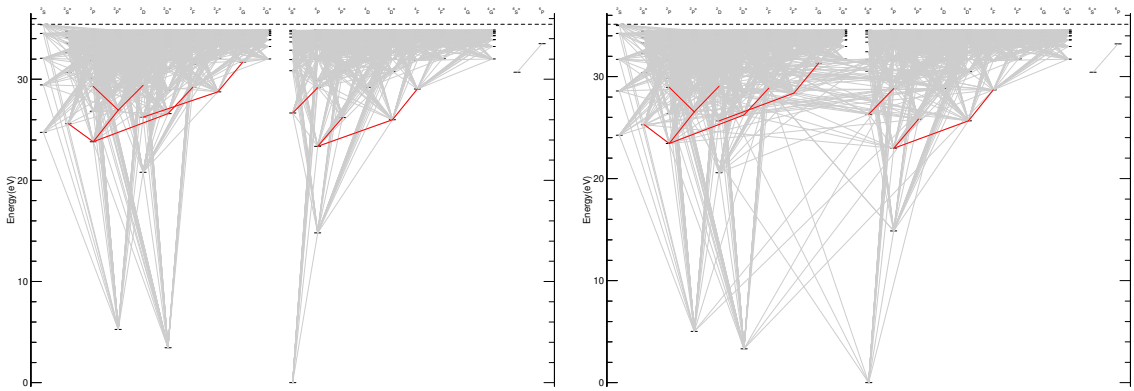

(a) *Model 1* **(b)** *Model 2*

Figure 3: *Grotrian diagrams of O* II *highlighting in red the radiative transitions corresponding to the multiplets summarized in Table 3*

5.3 Abundance calculation methodology

In the first place we must define quantitatively what do we understand by chemical abundance and the notation that will be used throughout the study. Due to historical reasons each field of astronomy counts with its own metrics. Nevertheless, in this work we will stick to the so called *astronomical scale*. In astronomy, the word *Abundance* usually refers to the ratio of its number density, $n(O)$, to that of hydrogen $n(H)$ (Stasinska G et al, 2012). Element abundance is often expressed on a logarithmic scale where the value for hydrogen is taken to be 12:

$$A(O) = log\epsilon(O) = log\frac{n(O)}{n(H)} + 12 \tag{19}$$

From now on any results concerning the abundance of oxygen, unless explicitly stated otherwise, will refer to the aforementioned quantity $A(O)$.

5.3.1 The curve of growth method

A stellar abundance analysis can be performed following to complementary approaches: *the curve of growth method* and the so-called *spectral synthesis method*. In this work, the complete analysis will be done following the former. The advantage of this method is that it allows the usage of line equivalent widths and to ignore any rotational or macroturbulent broadening mechanisms (Simón-Díaz, 2020). This section is dedicated to a careful explanation of the process of calculating chemical abundances, microturbulences and both of its associated uncertainties. For this study we made use of an IDL routine developed by Sergio Simón-Díaz which can carry the whole abundance analysis given that the set of equivalent widths measured from the grid of synthetic spectra described in Sect. 4.3 and the corresponding measurements as resulting from the observed spectrum be fed to it. The curves of growth have three distinct segments (Nahar, 2011).

1. *The linear part:* The equivalent width increases linearly with the number of ions N_i of element X in optically thin regions $\tau << 1$ as

$$EW \sim \tau_\nu \sim N_i \sim \frac{N_i}{N_X}\frac{N_X}{N_H}N_H \sim A_X \tag{20}$$

where A_X is the abundance ratio N_X/N_H

2. *The saturated part:* The saturation of the line profile happens when the density of ions is sufficient to absorb nearly all of the continuum energy at the center wavelength. At this points any increase in abundance results in an increase in equivalent width given by $EW \sim \sqrt{lnN_i}$

3. *The damped high-density part:* It occurs when the line profile at the core is saturated and ions start absorbing photons in the line wings. Equivalent width starts changing as $EW \sim \sqrt{N_i} \sim A_X^{1/2}$

In this study dealt with O II lines belonging to the linear section. Taking this into consideration, Fig. 4 shows the expected shape of the curves of growth obtained by plotting the theoretical equivalent width for each microturbulence versus the abundance . Then, for each line (and microturbulence) an abundance is derived from the observed equivalent width (and its error).

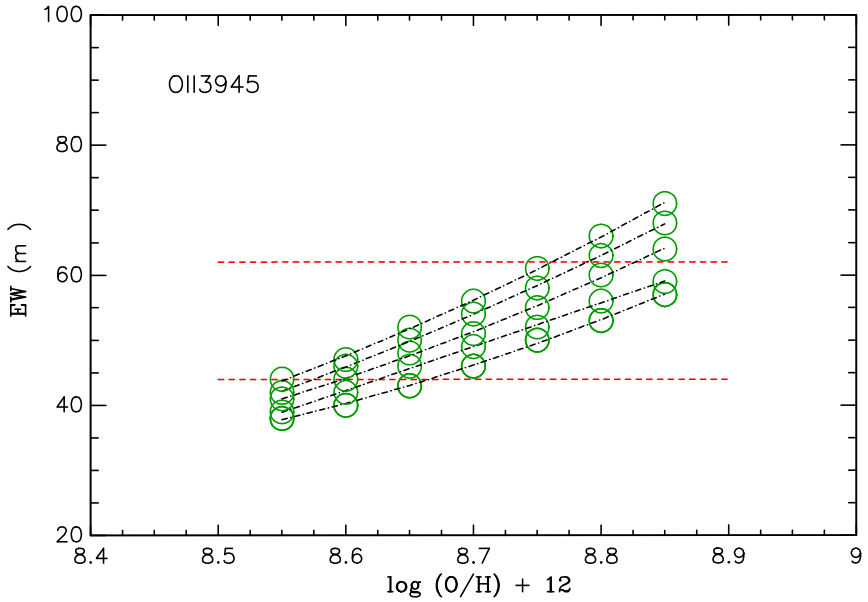

Figure 4: *Curves of growth for O II3945 line. Every curve corresponds to a different microturbulence increasing from bottom up (from 1 to 9 km/s in steps of 2 km/s). Dotted lines represent the uncertainty in the observed equivalent width.*

Next, in order to obtain the microturbulence, $log\epsilon - EW$ diagrams (Fig. 5) for every microturbulence in the model are obtained. The value that minimizes the dependence of line abundances in equivalent width (produces a zero slope) is chosen as the final microturbulence (Simón-Díaz, S, 2005). Uncertainties in this case arise from the errors derived from the slope (Which in turn come from errors in the individual line abundances).

Figure 6 shows the dependence of the slope on the the considered values of microturbulence which allows us to estimate the contribution of its uncertainty to that of the total oxygen abundance. It is worth noting that this uncertainty comes mainly from the quality of the spectra. The last step of the analysis is to calculate abundances and uncertainties for each line for the adopted microturbulence. The final abundance is calculated using a weighted mean of the linear individual abundances. Given that in this study we are primarily concerned with the line dispersion (in order to check the reliability of our model atoms) the uncertainty of the mean used is the standard deviation. There are, at least, four sources of error contributing to the final abundance uncertainty: those coming from the errors in the determined microturbulence, those referred to the stellar parameters, considered atomic data for the calculation of the synthetic spectrum and errors in the model atoms.

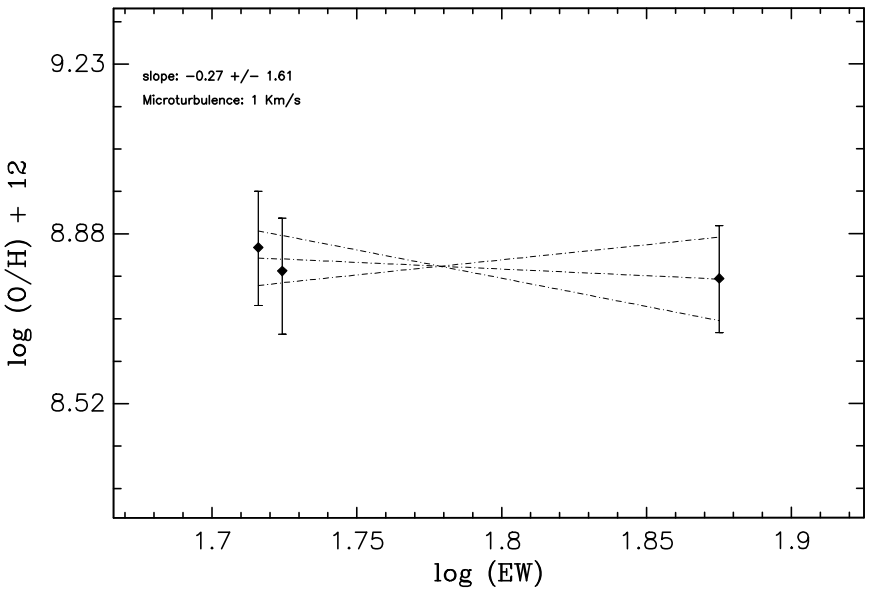

Figure 5: *logϵ - EW diagram for multiplet 3 for the microturbulence value producing an almost zero slope. In the graphic the calculated slope (and its error) are plotted in dotted lines.*

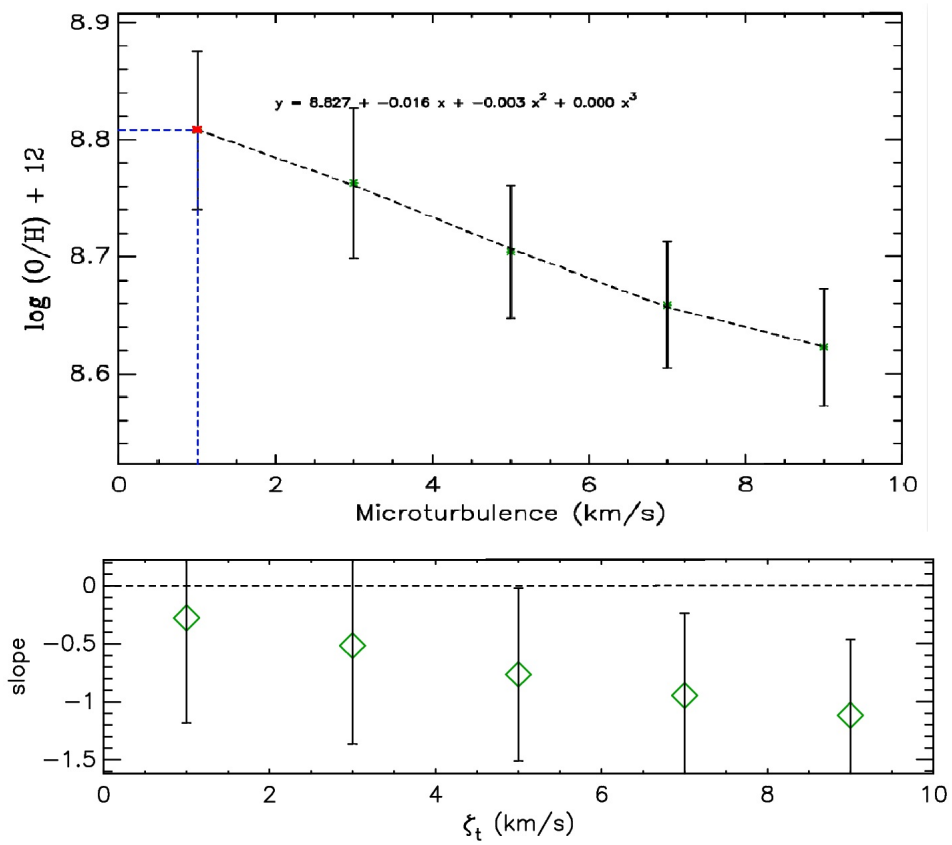

Figure 6: *(Top) Variation of abundance with microturbulence. (Bottom) variation of the slope with microturbulence. Both graphics are made for multiplet 3.*

5.3.2 Effect of Stellar parameters on Equivalent width

In the context of abundance analysis, chemical abundance itself is not the only physical quantity that plays a role in the shape and equivalent width of absorption lines. In a star there are many parameters that explain and characterize its processes. However, given the scope of this work only effective temperature, surface gravity and microturbulence will be considered explicitly to affect equivalent widths. This section will not only explain how these parameters affect equivalent widths but also give insights into how an erroneous determination of them could skew abundance results. As the primary objective of this work is to test two model atoms under the same conditions, the precise determination of the stellar parameters is not as crucial. As mentioned in section 3.3, the effective temperature and surface gravity calculated for the grid is not exactly the one derived by Gracía-Rojas et al. (2014). In that sense, it is important to review in what way the differences between the stellar parameters used and those derived could globally affect the outcome of the abundance analysis. The results presented in this section will be analysed in a general manner so they can be applied to others stars with different stellar parameters. In addition, some comments will be made on how an analysis of equivalent width as a function of effective temperature could be a useful tool in qualitatively detecting line contamination.

Effective Temperature In stellar astrophysics effective temperature is defined in terms of the total power per unit area radiated by the star

$$\int_0^\infty F_\nu d\nu = \sigma T_{eff}^4 \tag{21}$$

Effective temperature is the stellar parameter that most strongly affects line strength (Gray, 2008; see also, Fig. 7). A correct determination of this parameter is essential in any abundance analysis study. The temperature dependence of the absorption lines resides in the way level populations are affected by it. When a greater number of ions are in an specific state the probability of transitions associated to that level occurring rises. In order to illustrate that dependency we plotted EW against effective temperature for lines in multiplet 1 (see Table 3). These plots reveal the shape of the curve relating these two quantities and how an erroneous determination of $T_{\rm eff}$ can change the calculated ion abundance greatly. To create the figures in this Section, we used synthetic spectra from the BSTAR2006 grid from TLUSTY (Lanz and Hubeny, 2007) with microturbulence fixed to ξ_t=10 km/s, surface gravity to $log g = 3.00$ dex and effective temperature ranging from 15000K to 30000K in steps of 1000K

Figure 7 shows that, at least inside the same multiplet, the EW of a line presents a maximum surrounded by symmetric decline. This sensitivity is the main reason a careful determination of effective temperature is crucial when calculating abundances. The temperature dependence means that a deficient determination of effective temperature would move the curves of growth (i.e the ones from figure 4) up or down. Therefore, given that line abundances are calculated from those curves of growth, abundance results are also dependent on a reliable determination of effective temperature.

Surface gravity On the other hand, surface gravity also plays a role in the behaviour of spectral lines. Figure 8 shows the results of considering two different surface gravities but keeping the rest of the stellar parameters fixed. Again, a deficient determination of surface gravity will shift the curves of growth vertically and thus affecting the derived abundances.

Microturbulence It is evident from the square root dependence in the saturation part of the curve of growth that the slope is less there than in the other portions of the curve. This flattening

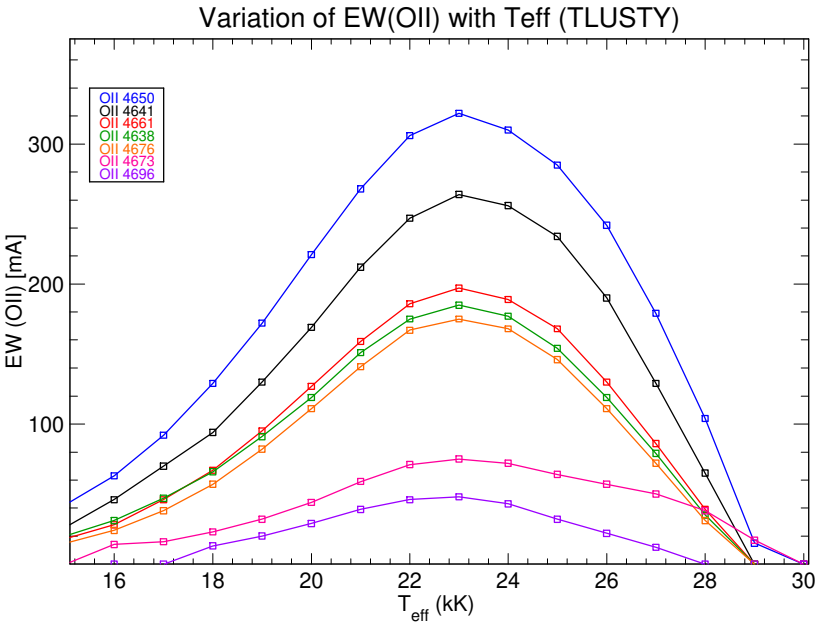

Figure 7: *Dependence of the EW of the O* II *lines from multiplet 1 (see Table 3) with the effective temperature.*

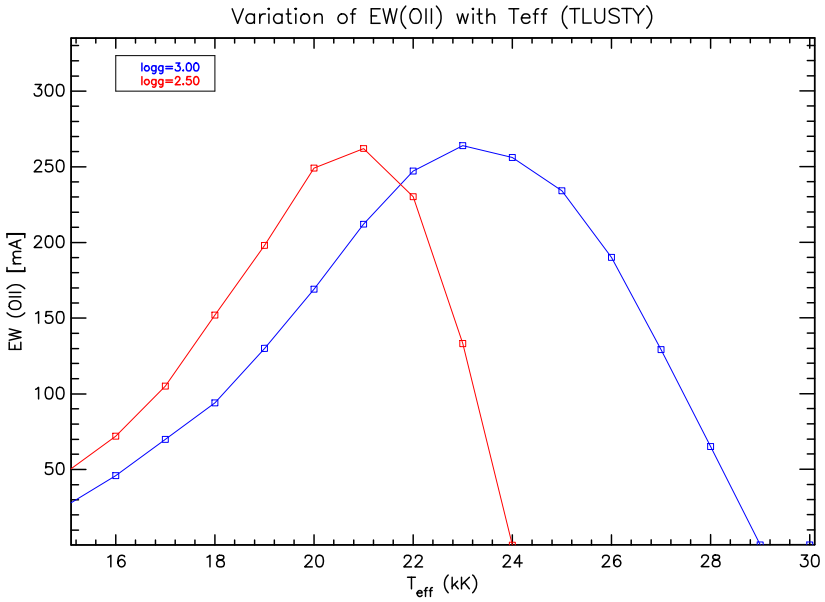

Figure 8: *EW vs T_eff of the O* II *4641 line from multiplet 1 (see Table 3) showing the results for two different values of surface gravity.*

has a very problematic effect, errors in equivalent widths account for much larger errors in abundance. So the correct treatment of lines in that range is imperative.

Microturbulence was incorporated into the abundance analyses to account for the fact that equivalent widths in the saturated part are greater than the ones predicted by models based on thermal and damping broadening alone (Gray, 2008). If microturbulence were not considered the abundance results for a given EW would be significantly larger aided by the small slope in this portion of the curve mentioned before. Microturbulence finds its physical interpretation in the small-scale mass motions compared to the unit optical depth taken as an isotropic Gaussian velocity distribu-

tion of dispersion ξ_t.

It is of importance to also note that microturbulence will not affect weaker lines as much as these are located in the linear portion of the curve. For weak lines increasing ξ broadens its Gaussian shape and produces a wider Gaussian with its equivalent width conserved. However, for lines in the saturated part a ξ increment widens the wavelength range covered by the line thus increasing the absorption and, consequently, the equivalent width. Figure 5 shows a cumulative frequency histogram showing how microturbulence shifts appreciably the strong lines to the right (increases their EW for the rest of parameters fixed) while the weaker lines are not affected as much.

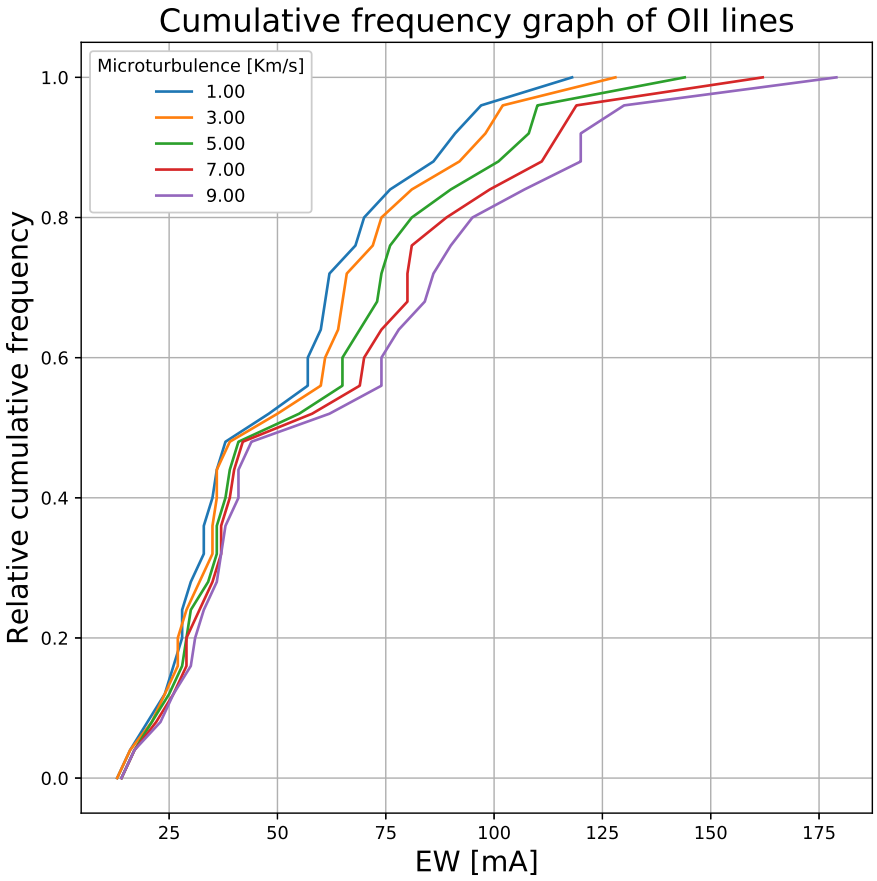

Figure 9: *Relative cumulative frequency graph of O* II *lines against equivalent width. Microturbulence reduces the slope of the graph meaning that the equivalent width of the lines increased. The difference in sensitivity of weak/strong lines is visible comparing the change at the start of the curve to the end. For this graph oxygen abundance was fixed to 8.85 dex*

5.3.3 Detection of line contamination using effective temperature dependence

EW vs. T_{eff} diagrams (like the ones presented in previous section; e.g. figure 7) are useful in visually recognizing contamination in a line for a given temperature. As the shape of the EW vs T_{eff} curve is expected to be the same for every line any curve behaving differently could be a sign of line contamination. So, it is imperative that any study regarding the degree of contamination of a line must be done with the T_{eff} correctly fixed. Contamination percentages calculated with two different temperatures are not expected to be equal. However, it is important to note again that

contamination may not be cause of the asymmetry. So, the real usefulness of these plots lies in that they can be used to quickly evaluate the behaviour of lines in different temperatures and pinpoint which of them require careful examination. Figure 10 shows an example of line with possible contamination the lower effective temperature range (The expected behaviour of absorption lines is shown in Fig. 7).

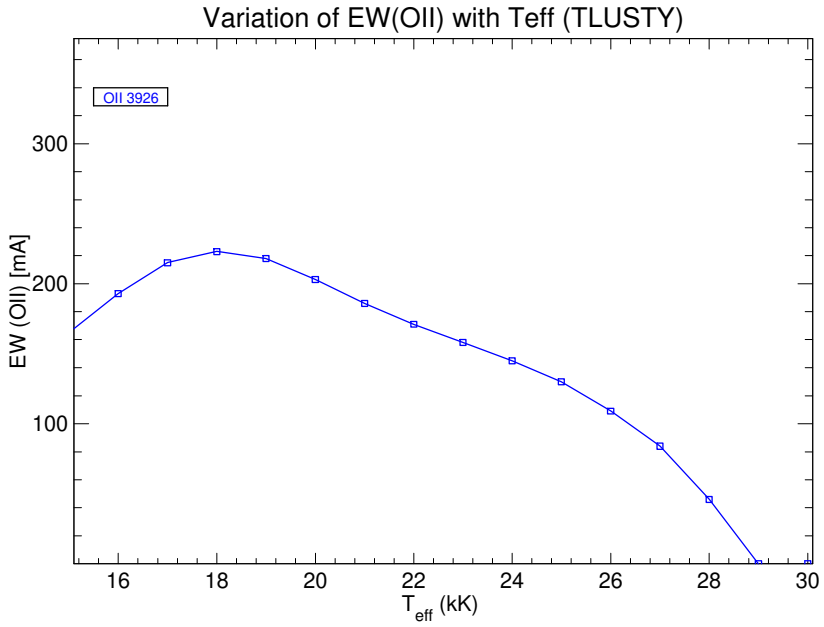

Figure 10: *The non-symmetry of the plot may indicate contamination of this line in that temperature range. Raising the EW*

6 Results

Finalmente los resultados principales de nuestro estudio son presentados en esta sección. En primer lugar se hace un análisis del resultado del estudio de abundancias con el conjunto completo de 46 líneas de diagnóstico para ambos modelos donde se comenta también sobre la diferencia en resultados de microturbulencias que arroja cada modelo. Luego se realiza un análisis de resultados separando las líneas por multipletes, haciendo un análisis de la sensibilidad de las líneas comparando sus abundancias entre modelos cuando la microturbulencia se mantiene fijada a un valor concreto. Por último, se dan las consideraciones globales sobre el resultado del análisis por multipletes.

In this section we present the results of our study based on the curve of growth method. First, we will select and discard lines that presented problems arising during the EW measurement of the observational spectra. Then, we will present the lines that must be discarded after a careful revision of their curves of growth. Following, the outcome of the complete abundance analysis for the two model atoms is presented and discussed in parallel in order to remark on its differences and similarities. Next, an analysis of the abundance results with the final set of O II divided by mutliplets is performed (see Sect. 6.3). Finally, those results are used to serve as the basis of the final discussion on the level of accuracy obtained derived from the use of different model atoms, thus fulfilling the main objective of this work. To test two different model atoms in the same physical conditions (i.e the same star).

6.1 Discarded Lines

The analysis carried out in Sect. 4.2 allowed us to select a preliminary set of O II lines. Still, measuring the equivalent widths in the observational spectra and plotting of the curves of growth proved to be useful in identifying further problematic lines not detected previously. This section will focus on a review of the lines that will be excluded from the final analysis.

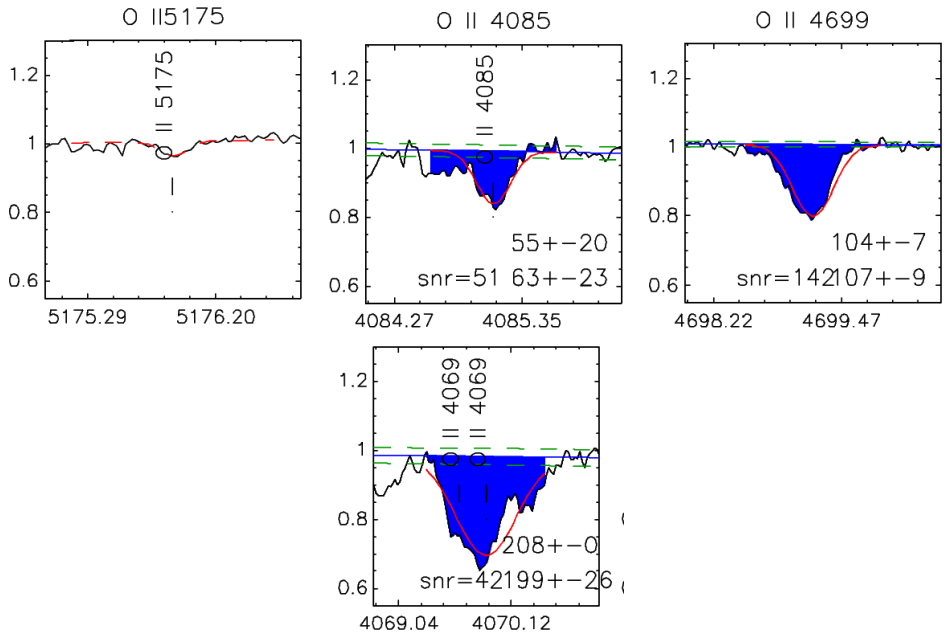

Figure 11: *Illustrative examples of the outcome of the EW measurement process in some problematic lines. Red line represents the Gaussian fit.*

Figure 11 show some cases of troublesome lines. For instance, the O II 5175 line is so faint that the procedure could not measure its equivalent width, hence it will be excluded from the final list of lines. O II 4086, on the other hand shows the contamination coming from O II 4084.65 (commented in Table 3) to be significant, making the line deviate from the expected Gaussian shape and thus deeming the EW measurement of the line inaccurate. Next, O II 4699 shows displacement of

its profile's peak from the expected position(maintaining, nonetheless, Gaussian shape), perhaps coming from a miscalculation of the center of the line or from a blend with the O II 4698.43 line (as well as contamination with Ne II 4698.43 line, mentioned in Table 3). Moreover, the equivalent width measurement of line O II 4069 is flawed. The shape of the line deviates greatly from the expected Gaussian shape mainly due to the poor signal to noise ratio in that region of the spectrum but also to some contamination not considered before which broadens the wings of the lines and causes the EW to rise. O II 4069 is therefore discarded from the study. All of these four lines will be therefore discarded and not be included in the final list of lines.

Checking the curves of growth showed to be useful as well in this first approach; lines of multiplet 12 (O II 5160, O II 5190 and O II 5207) were found to be wrongly modelled when the curves of growth plotted (Fig 12) did not follow the expected behaviour presented in the section 5.3.1. Bearing this in mind the whole multiplet is then removed from the study.

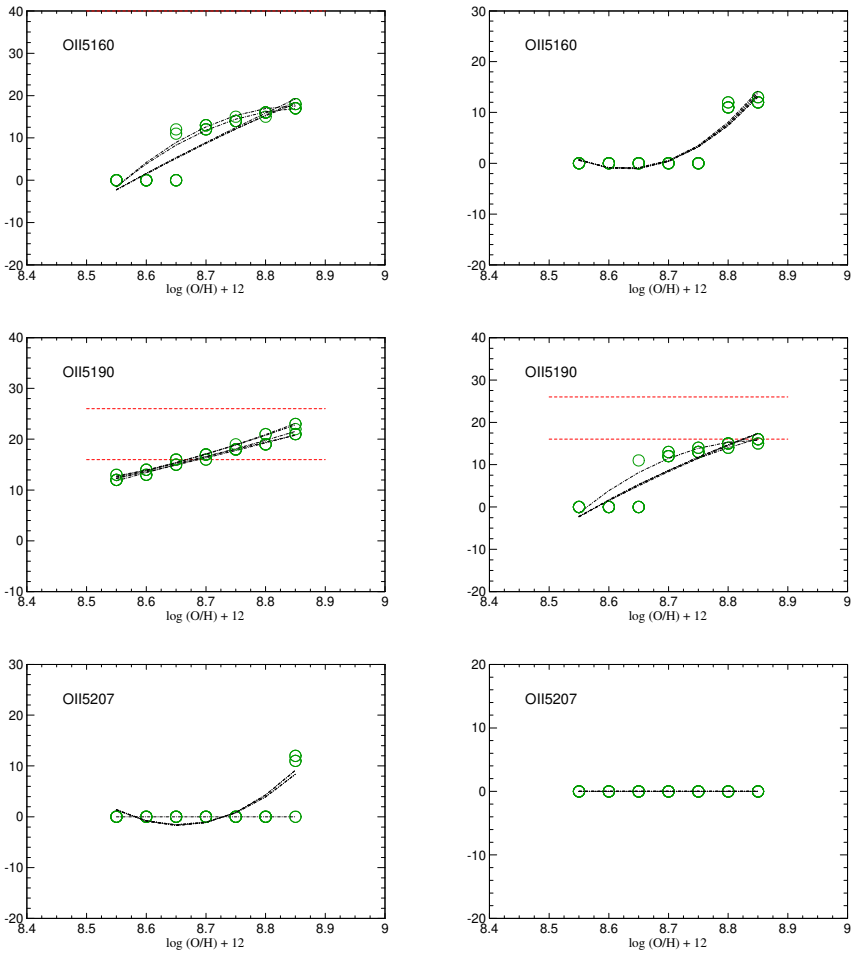

Figure 12: *Curves of Growth of lines in multiplet 12 exhibiting a behaviour which indicates the existence of an error in the modelling process for both models. Model 1 (Left) and Model 2 (Right).*

6.2 Abundance Calculation

After completing the filtering process of the preliminary set of diagnostic lines in the previous section and having excluded already seven problematic lines in Sect 6.1, we hereby present the final set of O II absorption lines in Table 13. Using this final set of lines, we performed an abundance analysis using the two versions of the O II model atoms specifically built for this work.

The results of this analysis are presented in this section, were we separate the case in which all lines are analyzed together (see Fig. 13) and separately by multiplets (see Sect. 6.3). In this section we will analyse the difference in results between the two models in two situations. First, when the microturbulence used correspond to the one giving the zero slope fit for each model and then when its fixed to a certain value for both models simultaneously.

Multiplet	Line
1	O II 4650, 4661, 4638, 4676, 4696
2	O II 4349, 4317, 4319
3	O II 3954, 3982, 3945
4	O II 6721, 6641
5	O II 4414, 4416, 4452
6	O II 4590, 4596
7	O II 4072, 4078
8	O II 4705
9	O II 4924, 4906, 4891
10	O II 4943, 4956
12	O II 4185, 4189

Table 4: *Final set of lines.*

The results of obtained by the consideration of the two O II model atoms (summarized in Table 5) show good agreement with the oxygen abundance derived by García-Rojas et al. (2014). In addition, the results between models are in good agreement (taking into account the associated uncertainties). Model 1, however, appears to throw a more reliable results considering it produces a lower dispersion in the individual line abundances. The zero slope fit in the log(O/H)+12 vs log(EW) plot was reached for two different microturbulences (3 km/s in model 1 and 5 km/s in model 2).

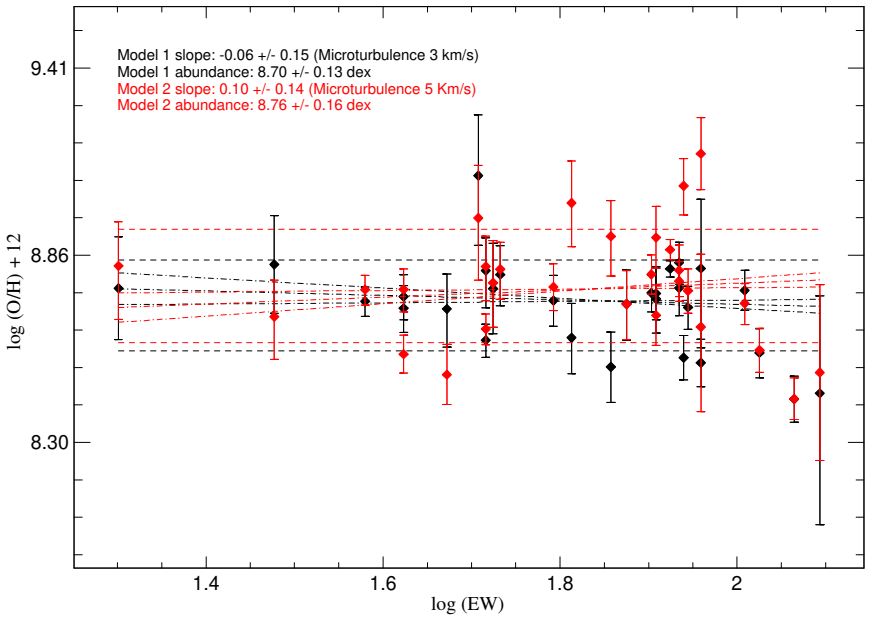

Figure 13: *Abundance results corresponding to the zero slope fit for model 1 (black) and model 2(red).*

Figure 14 shows the resulting differences in the derived line-by-line abundances between both analysis when the microturbulence is fixed to 3 and 5 km/s, respectively. It is shown that the majority of lines in model 2 present a higher abundance than their model 1 counterparts. Detailed discussion of the results of individual lines and multiplets is given in the next section.

Final set		
	Abundance [*dex*]	Microturbulence
Model 1	8.70 ± 0.13	3 km/s
Model 2	8.76 ± 0.16	5 km/s

Table 5: *Abundance results corresponding to the zero slope fit for each model.*

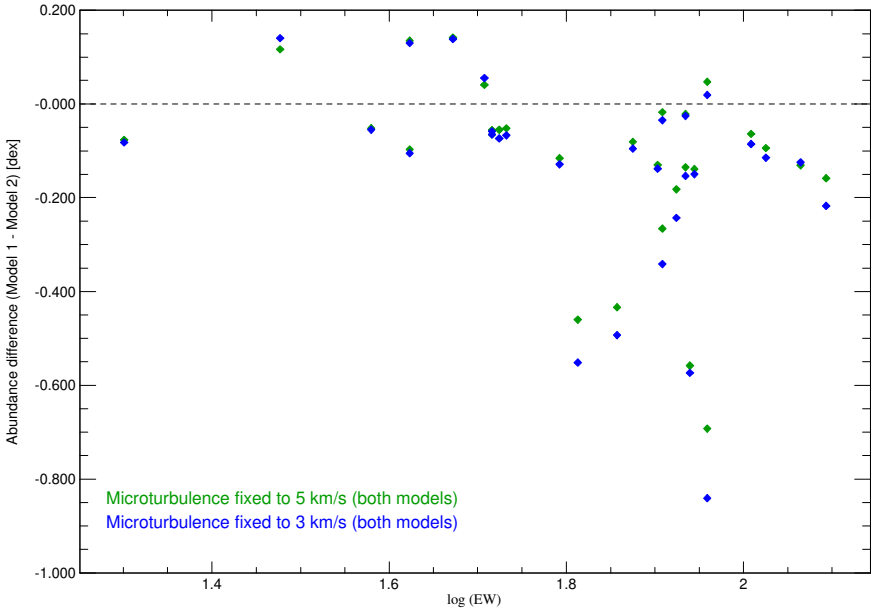

Figure 14: *line-by-line abundance difference (Model 1 - Model 2) using a fixed microturbulence. In green results corresponding to ξ_t=5 km/s and in blue results corresponding to ξ_t= 3 km/s.*

6.3 Multiplet Analysis

In order to minimize the effect of line abundance dispersion in the microturbulence determination, the set of lines used should ideally span a large range of EWs. In the case of O II, specifically, lines coming from the same multiplet have only a small range of equivalent width; so the use of different multiplets simultaneously is a necessity. In consequence, the unavoidable use of several multiplets will contribute to derive a (more) accurate value for microturbulence. There is interest as well, from the point of view of model atom testing, in studying multiplets individually. Lines from the same multiplet come from sublevels grouped together in the model calculation. If an error in the calculation is made this would produce an error in the global transition, and hence in the lines within this multiplet with respect to other multiplets. Given that the miscalculation is of a global nature lines that, within one multiplet, throw abundance much higher/lower than the mean of the multiplet could be suffering from errors coming directly from the atomic data used for its calculation. In conclusion, multiplet analysis proves to be useful in finding deficiencies in the model atoms not apparent when the full abundance calculation is made.

The individual multiplet analysis will be carried out in several parts. First, we will compare the abundance of the lines of the multiplet against the mean in both models. Next, we will calculate the difference in resulting line-by-line abundance between model atoms when the microturbulence is fixed to a certain value (3 km/s and 5 km/s). This comparison is made with the idea of finding which lines are more sensitive to changes in model atom. Those lines in a given multiplet providing results far from the mean abundance in both models are likely to have problems concerning the considered atomic data. Finally, we will also take into account that line dispersion within the multiplet is another likely indicator of problems regarding the atomic data and not the model atom itself.

Multiplet	EW range (mÅ)
1	98
5	52
10	42
7	40
3	23
9	17
4	14
12	7
2	5
6	4

Table 6: *Multiplets ordered by EW range. Multiplets with a larger range are preferred over those with a low range for a more accurate microturbulence determination which, as said in section 3.1 affects the abundance calculation as well.*

6.3.1 Specific individual notes for all considered multiplets.

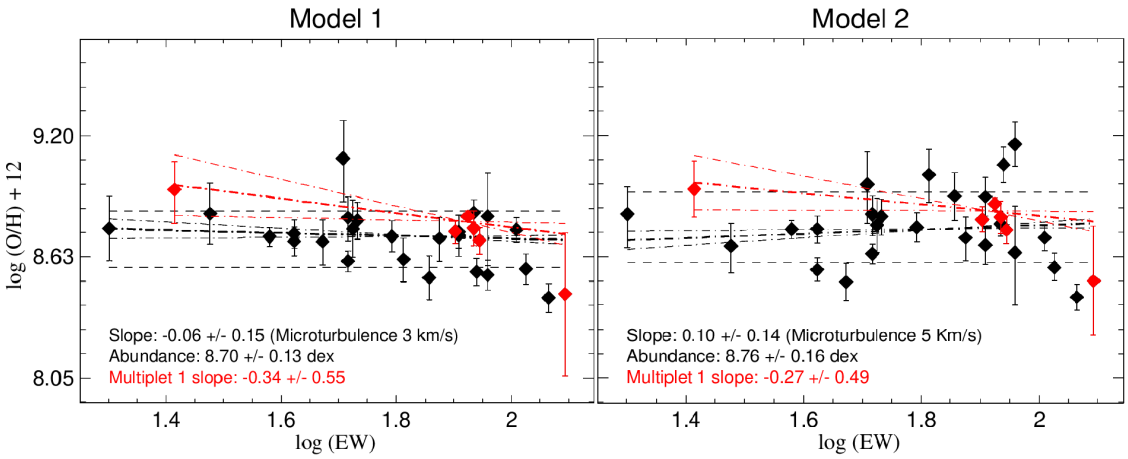

Figure 15: *logϵ − EW plot highlighting Multiplet 1*

Line	EW [mÅ]	A(O) [dex]				ΔA(O) (M1-M2) [dex]	
		(M1, $\xi_t = 3$)	(M1, $\xi_t = 5$)	(M2, $\xi_t = 3$)	(M2, $\xi_t = 5$)	($\xi_t = 3$)	($\xi_t = 5$)
OII4650	124 ± 29	8.45 ± 0.34	8.35 ± 0.22	8.67 ± 0.31	8.51 ± 0.26	−0.22	−0.16
OII4661	88 ± 6	8.70 ± 0.06	8.61 ± 0.06	8.85 ± 0.07	8.75 ± 0.07	−0.15	−0.14
OII4638	86 ± 7	8.76 ± 0.08	8.68 ± 0.07	8.92 ± 0.08	8.81 ± 0.08	−0.16	−0.13
OII4641	84 ± 2	8.82 ± 0.02	8.69 ± 0.03	9.06 ± 0.03	8.87 ± 0.03	−0.24	−0.18
OII4676	80 ± 5	8.75 ± 0.05	8.67 ± 0.05	8.89 ± 0.06	8.80 ± 0.06	−0.14	−0.13
OII4696	26 ± 7	8.95 ± 0.15	8.94 ± 0.15	8.96 ± 0.14	8.95 ± 0.13	−0.01	−0.01

Table 7: *Summary of EW measurements and derived oxygen abundances resulting from curve of growth analysis using Model 1 (M1) and Model 2 (M2) for multiplet 1. Note that the quoted abundances for individual lines correspond to the microturbulence producing a zero slope in the A(O)-log(EW) diagram when all lines are considered (i.e. 3 and 5 km s^{-1}, for Model 1 and Model 2, respectively). For comparison purposes, the last two columns show the difference between the individual line-by-line abundances resulting from the analysis performed with each of the considered atomic model with microturbulence fixed to 3 km/s and 5 km/s respectively.*

Multiplet 1 (Fig 15 and Table 7).

- O II 4650 presents the lowest abundance (and highest uncertainty) of the multiplet in both models. The line is also the second most sensitive to model atom changes within the multiplet. The low abundance in both models points to a problem with the considered atomic

data. Possibly the log(gf) value (0.43) considered in our formal solution computations (with Synspec) is too high. Interestingly, the value proposed by the atomic line list (0.32, see Table 3) could help to solve the problem with this line.

- O II 4696, on the other hand, is the less sensitive of the multiplet (-0.01 dex difference for both microturbulences). Furthermore, the line abundance is well above the mean in both models. The high abundance presented in both models could point to a problem regarding the log(gf) value used for calculating the synthetic spectra. A line with lower log(gf) value needs more abundance to replicate an equivalent width. In that sense we know also that for this line the atomic line list presents an even lower log(gf) value than the one used for our synthetic grid calculation (Table 3). Hence, both log(gf) values should be revised.
- O II 4641 is the most sensitive to model atom changes. Its abundance its within the uncertainty of the mean in both models.
- O II 4661, O II 4638, and O II 4676 all return abundances inside the uncertainty of the mean and show a similar degree of sensitivity to model atom changes. These lines appear to be well behaved for abundance analysis in both model atoms.
- The slopes of the multiplet vary slightly between models (mainly because of the lower abundance of O II 4650 in model 1 pulling the slope down) but are still within the uncertainties of each other. It is important to remark as well that this multiplet is the one with the largest EW range, so its use for microturbulence determination is very much recommended.

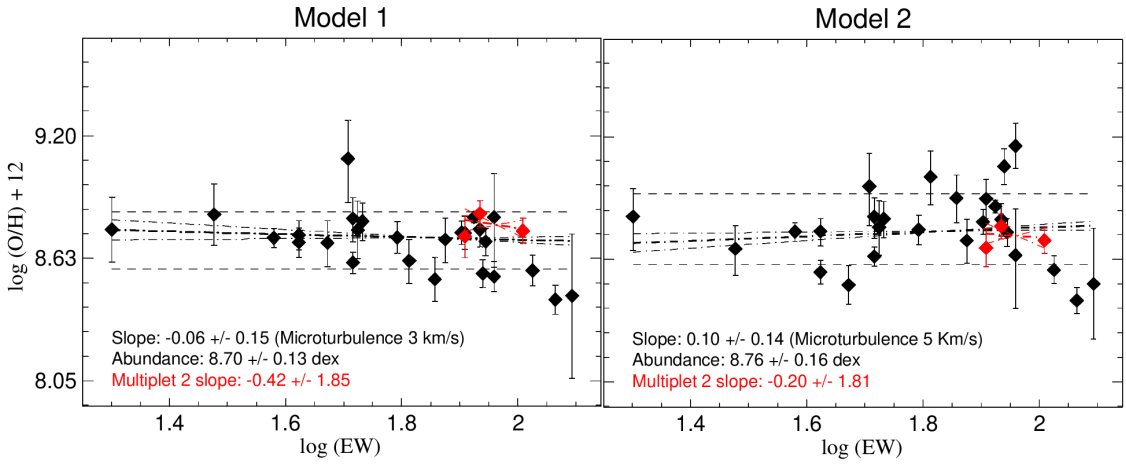

Figure 16: *$A(O) - EW$ plot highlighting Multiplet 2*

Line	EW [mÅ]	A(O) [dex]				ΔA(O) (M1-M2) [dex]	
		(M1, $\xi_t = 3$)	(M1, $\xi_t = 5$)	(M2, $\xi_t = 3$)	(M2, $\xi_t = 5$)	($\xi_t = 3$)	($\xi_t = 5$)
OII4349	102 ± 6	8.75 ± 0.06	8.65 ± 0.05	8.84 ± 0.06	8.72 ± 0.06	-0.09	-0.07
OII4319	86 ± 6	8.84 ± 0.06	8.76 ± 0.06	8.86 ± 0.06	8.78 ± 0.06	-0.02	-0.02
OII4317	81 ± 8	8.73 ± 0.10	8.66 ± 0.09	8.76 ± 0.10	8.68 ± 0.09	-0.03	-0.02

Table 8: *Results for multiplet 2*

Multiplet 2 (Fig 16 and Table 8).

- Every line in the multiplet (for model 1 and 2) is inside the σ dispersion associated with the mean value of abundances. So, there is no reason (Using *only* the abundance results as reference) to assert that one model behaves better than other.
- Line O II 4319 presents higher abundance to the rest of the lines of the multiplet in both models pointing to problems in the model considered atomic data, possible a log(gf) value moderately low. This line, along with O II 4317, are not much sensitive to model atom changes.

- Line O II 4349 is the most sensitive line to model atoms.

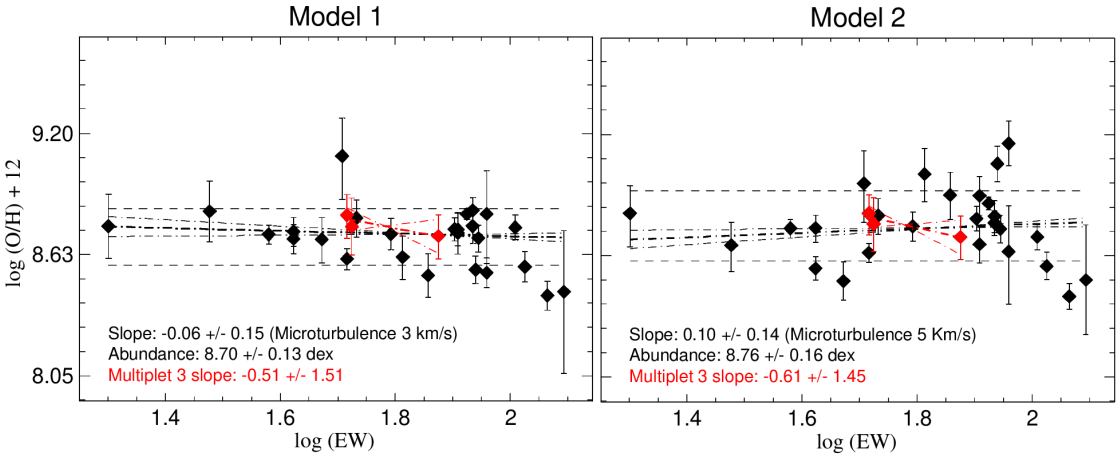

Figure 17: *$A(O) - EW$ plot highlighting Multiplet 3*

Line	EW [mÅ]	A(O) [dex]				ΔA(O) (M1-M2) [dex]	
		(M1, $\xi_t = 3$)	(M1, $\xi_t = 5$)	(M2, $\xi_t = 3$)	(M2, $\xi_t = 5$)	($\xi_t = 3$)	($\xi_t = 5$)
OII3954	75 ± 8	8.71 ± 0.10	8.63 ± 0.09	8.81 ± 0.12	8.71 ± 0.10	-0.10	-0.08
OII3945	53 ± 9	8.76 ± 0.13	8.72 ± 0.11	8.83 ± 0.15	8.78 ± 0.13	-0.07	-0.06
OII3982	52 ± 8	8.81 ± 0.10	8.77 ± 0.09	8.87 ± 0.11	8.83 ± 0.10	-0.06	-0.06

Table 9: *Results for multiplet 3*

Multiplet 3 (Fig 17 and Table 9).

- Line O II 3954 appears to be susceptible to model atom changes.
- The slope value remains almost the same across models suggesting that the dispersion between lines within the multiplet is probably caused by faulty $\log(gf)$ values.
- The low sensitivity of this multiplet to model atom changes make it to be a good candidate for calibration of atomic data.

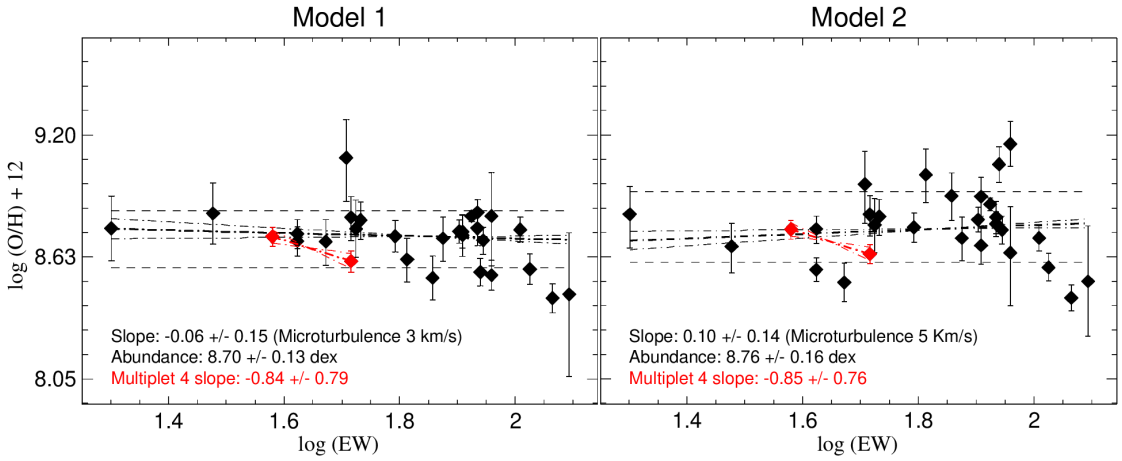

Figure 18: *$A(O) - EW$ plot highlighting Multiplet 4*

Line	EW [mÅ]	A(O) [dex]				ΔA(O) (M1-M2) [dex]	
		(M1, $\xi_t = 3$)	(M1, $\xi_t = 5$)	(M2, $\xi_t = 3$)	(M2, $\xi_t = 5$)	($\xi_t = 3$)	($\xi_t = 5$)
OII6721	52 ± 4	8.61 ± 0.05	8.58 ± 0.04	8.67 ± 0.05	8.64 ± 0.04	-0.06	-0.06
OII6641	38 ± 3	8.72 ± 0.04	8.70 ± 0.04	8.78 ± 0.04	8.76 ± 0.04	-0.06	-0.06

Table 10: *Results for multiplet 4*

Multiplet 4 (Fig 18 and Table 10).

- In this multiplet the susceptibility to the model atom used is not the dependent on microturbulence. The abundance difference between models is the same for both microturbulences considered.
- O II 6721 is slightly lower in abundance than the other line in the multiplet in both models (especially in model 2). In this case we consider the line O II 6721 to be the one skewing the slope results since the other line (O II 6641) is much closer to the mean in both models. Therefore, we suggest that there must be some underlying problem with the considered atomic data for line O II 6721.

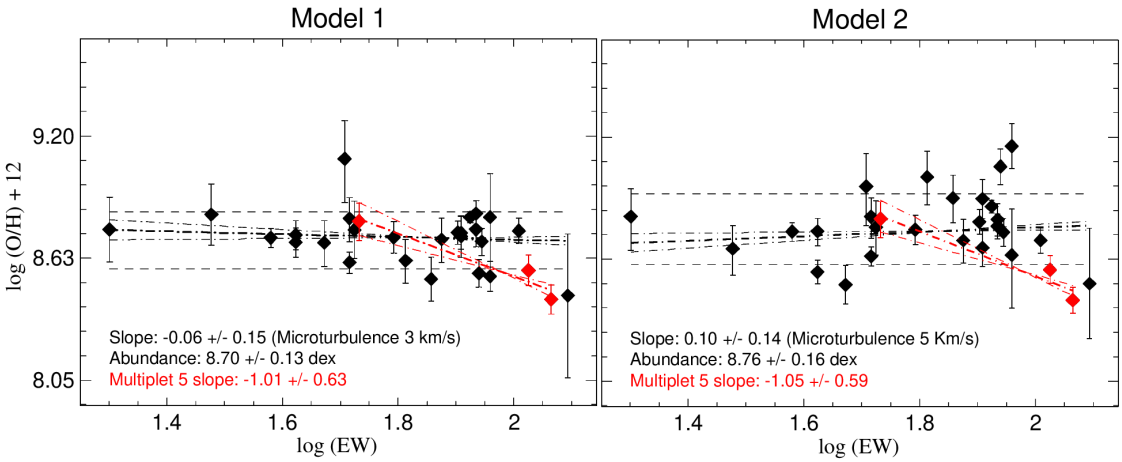

Figure 19: *$A(O) - EW$ plot highlighting Multiplet 5*

Line	EW [mÅ]	A(O) [dex]				ΔA(O) (M1-M2) [dex]	
		(M1, $\xi_t = 3$)	(M1, $\xi_t = 5$)	(M2, $\xi_t = 3$)	(M2, $\xi_t = 5$)	($\xi_t = 3$)	($\xi_t = 5$)
OII4414	116 ± 7	8.43 ± 0.07	8.30 ± 0.06	8.56 ± 0.08	8.43 ± 0.06	-0.13	-0.13
OII4416	106 ± 7	8.57 ± 0.07	$8.48 \pm .06$	8.68 ± 0.08	8.58 ± 0.07	-0.11	-0.10
OII4452	54 ± 7	8.80 ± 0.09	8.77 ± 0.09	8.87 ± 0.10	8.82 ± 0.08	-0.07	-0.05

Table 11: *Results for multiplet 5*

Multiplet 5 (Fig 19 and Table 11).

- Line O II 4414 is the most sensitive of the multiplet to model atom changes. The line also throws the lowest abundance value of all lines in the set for both models. There must be a problem with the underlying atomic data. The $\log(gf)$ value chosen for the formal solution computations appears to be too high. Therefore, we recommend using the $\log(gf)$ value coming from the atomic line list (see Table 3)
- The O II 4416 is also somewhat sensitive to model atom changes. Moreover, the abundance results are very low in both models. Again we recommend using the lower $\log(gf)$ value from the atomic line list instead of the higher one used for the synthetic spectra (see Table 3)
- In contrast, the O II 4452 throws abundance results above the mean in both models. The results however seem to be better in model 2.

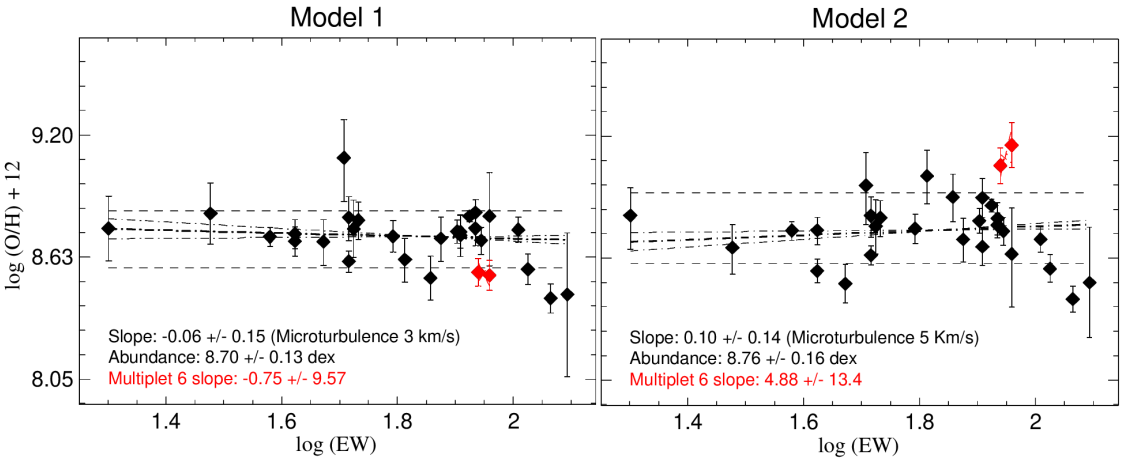

Figure 20: *$A(O) - EW$ plot highlighting Multiplet 6*

- The slope is almost the same in both models. Showing again that the dispersion within the multiplet must not be caused by the model atoms themselves.

Line	EW [mÅ]	A(O) [dex]				ΔA(O) (M1-M2) [dex]	
		(M1, $\xi_t = 3$)	(M1, $\xi_t = 5$)	(M2, $\xi_t = 3$)	(M2, $\xi_t = 5$)	($\xi_t = 3$)	($\xi_t = 5$)
OII4590	91 ± 7	8.54 ± 0.07	8.47 ± 0.06	9.38 ± 0.13	9.16 ± 0.11	-0.84	-0.69
OII4596	87 ± 8	8.55 ± 0.07	8.51 ± 0.06	9.13 ± 0.08	9.06 ± 0.08	-0.58	-0.55

Table 12: *Results for multiplet 6*

Multiplet 6 (Fig 20 and Table 12).

- This multiplet presents the most sensitive behaviour to model atom changes of the set, with the O II 4590 line being the most sensitive.
- Both line abundances in model 1 are within the uncertainty of the mean. In contrast the abundance results in model 2 for both lines are well above the mean.
- Taking into account both slope and line abundance results we conclude that this multiplet behaves better in model 1.
- The small EW range and sensitivity to changes in model atoms forces us to not recommend using this multiplet to neither microturbulence determination nor abundance calculations. However, it is also true that the aforementioned sensitivity could be be used to our advantage to test a new model atom against a reliable set of lines by fitting the results of this multiplet to the results from the reference set.

Line	EW [mÅ]	A(O) [dex]				ΔA(O) (M1-M2) [dex]	
		(M1, $\xi_t = 3$)	(M1, $\xi_t = 5$)	(M2, $\xi_t = 3$)	(M2, $\xi_t = 5$)	($\xi_t = 3$)	($\xi_t = 5$)
OII4072	91 ± 17	8.82 ± 0.22	8.69 ± 0.20	8.80 ± 0.26	8.65 ± 0.23	0.02	0.04
OII4078	51 ± 13	9.09 ± 0.19	9.01 ± 0.16	9.04 ± 0.21	8.97 ± 0.17	0.05	0.04

Table 13: *Results for multiplet 7*

Multiplet 7 (Fig 21 and Table 13).

- This multiplet, along with multiplet 9, is the only mutiplet where the abundance results are higher for model 1 for both microturbulences.

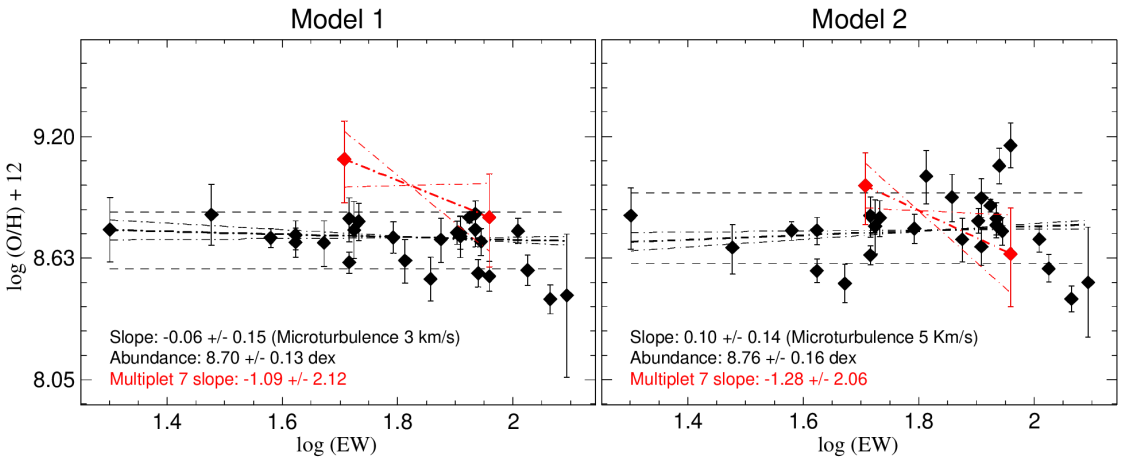

Figure 21: *$A(O) - EW$ plot highlighting Multiplet 7*

- The result of line O II 4072 is worth noting given that, in contrast with O II 4078 which somewhat conserves it position relative to the mean, its abundance results are higher than the mean in model 1 and lower in model 2.
- Considering that the O II 4072 abundance results relative to the mean (0.12 dex in model 1 and -0.11 dex in model 2) are similar in both models there is no way for us to assert the reliability of the line other than to compare them with those of the other line within the multiplet, in which case model 1 seems to throw slightly better results (less pronounced slope).
- Line O II 4078, yields results above the mean in both models so a problem with the atomic data is not discarded. The $\log(gf)$ value of -1.46 used for the synthetic spectra calculation appears to be too low. We recommend using the $\log(gf)$ value coming from the atomic line list of -0.29.

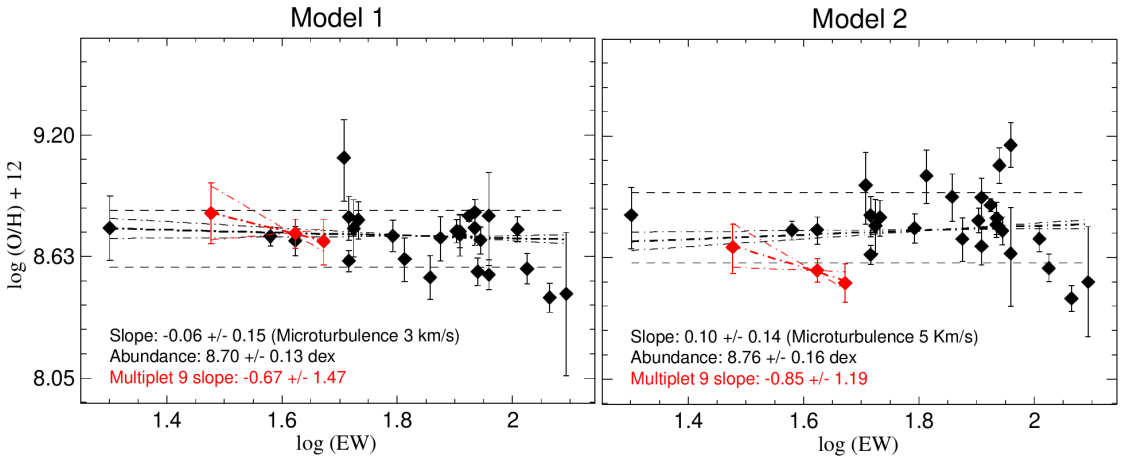

Figure 22: *$A(O) - EW$ plot highlighting Multiplet 9*

Line	EW [mÅ]	A(O) [dex]				ΔA(O) (M1-M2) [dex]	
		(M1, $\xi_t = 3$)	(M1, $\xi_t = 5$)	(M2, $\xi_t = 3$)	(M2, $\xi_t = 5$)	($\xi_t = 3$)	($\xi_t = 5$)
OII4924	47 ± 7	8.70 ± 0.11	8.65 ± 0.10	8.56 ± 0.10	8.51 ± 0.09	0.14	0.14
OII4906	42 ± 4	8.74 ± 0.07	8.70 ± 0.07	8.61 ± 0.07	8.57 ± 0.06	0.13	0.13
OII4891	30 ± 6	8.83 ± 0.14	8.79 ± 0.12	8.69 ± 0.12	8.68 ± 0.12	0.14	0.11

Table 14: *Results for multiplet 9*

Multiplet 9 (Fig 22 and Table 14).

- All lines in this multiplet are sensitive to model atom changes. The sensitivity seem to be somewhat correlated to line strength within the multiplet. Stronger lines present higher abundance difference.
- This multiplet, along with multiplet 7, are the only multiplets where the abundance is higher for model 1 for both microturbulences. This results points to a miscalculation of the level populations for these multiplets in model 1. The abundance results, nonetheless, are much closer to the mean in model 1.
- In model 1 all lines are above the mean, in contrast with model 2 where all lines are well below.
- This multiplet is also a good candidate to model atom calibration due to its high sensitivity.

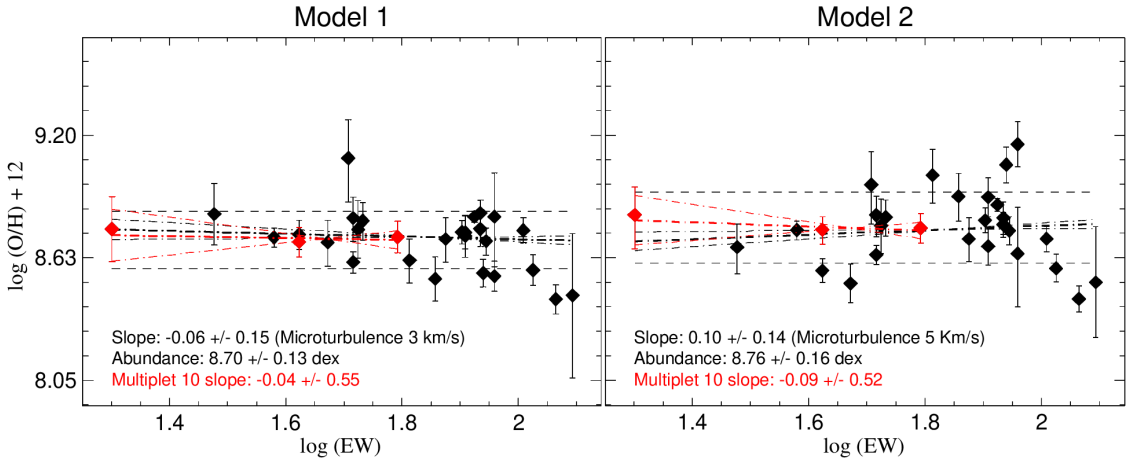

Figure 23: *$A(O) - EW$ plot highlighting Multiplet 10*

Line	EW [mÅ]	A(O) [dex]				ΔA(O) (M1-M2) [dex]	
		(M1, $\xi_t = 3$)	(M1, $\xi_t = 5$)	(M2, $\xi_t = 3$)	(M2, $\xi_t = 5$)	($\xi_t = 3$)	($\xi_t = 5$)
OII4943	62 ± 5	8.72 ± 0.08	8.65 ± 0.07	8.85 ± 0.08	8.76 ± 0.07	-0.13	-0.11
OII4941	42 ± 4	8.70 ± 0.07	8.66 ± 0.06	8.81 ± 0.07	8.76 ± 0.06	-0.11	-0.10
OII4956	20 ± 5	8.76 ± 0.15	8.75 ± 0.14	8.84 ± 0.17	8.83 ± 0.15	-0.08	-0.08

Table 15: *Results for multiplet 10*

Multiplet 10 (Fig 23 and Table 15).

- There appear to exist the same correlation with EW compared to the multiplet 9. Stronger lines in the multiplet are more sensitive to model atoms.
- All lines in the multiplet (for both models) are within the uncertainty of the mean. Line O II 4956 is slightly above the mean in model 2.
- The use of this multiplet is recommended to derive the oxygen abundance in a star and for abundance and microturbulence determination due to its good results across models, high EW range and low slope.

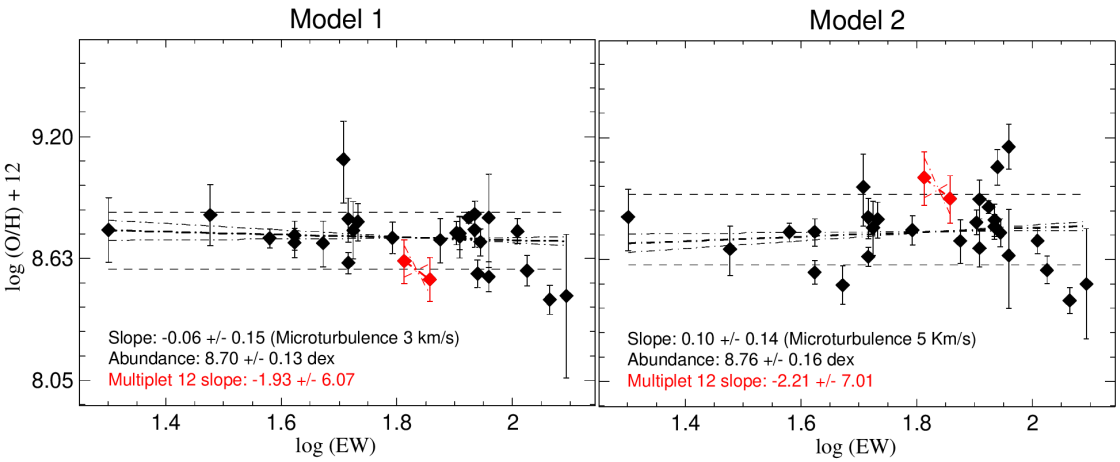

Figure 24: *$A(O) - EW$ plot highlighting Multiplet 12*

Line	EW [mÅ]	A(O) [dex]				ΔA(O) (M1-M2) [dex]	
		(M1, $\xi_t = 3$)	(M1, $\xi_t = 5$)	(M2, $\xi_t = 3$)	(M2, $\xi_t = 5$)	($\xi_t = 3$)	($\xi_t = 5$)
OII4189	72 ± 9	8.53 ± 0.10	8.48 ± 0.09	9.02 ± 0.13	8.91 ± 0.11	-0.49	-0.43
OII4185	65 ± 8	8.61 ± 0.10	8.55 ± 0.09	9.17 ± 0.17	9.01 ± 0.13	-0.56	-0.46

Table 16: *Results for multiplet 12*

Multiplet 12 (Fig. 24 and Table 16).

- The sensitivity of this multiplet to model atoms is evident in the fact that its mean abundance jumps from below the mean (in model 1) to above the mean (in model 2).
- The slope remains around the same value for both models, so the dispersion within the multiplet appears to be independent of the model atom used.
- The high sensitivity to model atoms and low EW range make this multiplet unreliable for both abundance and microturbulence determination.

6.3.2 Final Remarks

After the individual multiplet analysis some final remarks could be made summarizing the general behavior of the whole set of lines:

- There appears to be a bigger difference in abundance for strong lines than in weak ones.
- The abundance difference line by line is dependent on the microturbulence used. The abundance difference was higher for every line in the set for ξ_t=3 km/s than for ξ_t=5 km/s.
- Multiplet 6 and 12 are not recommended for abundance studies due to their high sensitivity to model atom changes. However, they are interesting candidates to test the model atoms against a reference set of lines with proven reliability.
- Multiplet 10 seems to be the most reliable of the set due to the abundance results compared to the mean and the small slope in both models. Also, its robustness against model atom changes make the multiplet a good fit to test atomic data.
- The comparison of two model atoms could serve, given that the right multiplets are chosen, as a framework to find problems in the atomic data used. The recommendation is to use multiplets which are less sensitive to changes in the model atoms. In our set multiplet 2 and 7 serve as good examples.

7 Conclusions

En esta sección se presentan las conclusiones finales del texto. Se recuerda que el objetivo de este trabajo no era dar un respuesta definitiva a cual de los dos modelos atómicos es mejor. En cambio, el objetivo era testear los modelos para comprobar su fiabilidad, encontrar errores en la información atómica considerada, desarrollar una metodología para futuros proyectos y estudiar el grado de sensibilidad de ls líneas al cambio de modelos atómicos. En este sentido, según las discusiones del capítulo anterior, se considera finalmente que la metodología seguida es satisfactoria y aplicable a futuros testeos de modelos atómicos sobre estrellas del mismo tipo espectral.

The primary focus of this study was to test two different O II model atoms by performing an oxygen abundance analysis (based on the curve of growth method) of the narrow line B0.5 V star BD+463474. It is worth mentioning again that the tests were not to explicitly reach a final conclusion of which of the model atom was the most precise of the two but to develop a methodology for the comparison, find problematic lines and suggest possible origins for said problems. To try to give a definite answer on the matter lies far beyond the scope of our study. Having that in mind, the results showed how the calculated abundance was lower for all but five lines in Model 1 causing the mean abundance to also be lower than Model 2. Moreover, the comparison also served to give a qualitative measure of the sensitivity of multiplets to model atom changes and identify problems in specific lines that could possibly indicate errors in the model atmosphere's atomic data. In that sense, the third objective of this work was to establish the framework in which to test model atoms using quantitative spectroscopic tools. However, at this stage, it is still to premature to assert which of the two considered model atoms is better. Nonetheless, this work has served to identify some problematic lines to be studied more in detail. Also, this pilot study has served to define a *methodology* which could be further replicated for another star, chemical species or set of model atoms.

In addition, a complete review was made on the dependence the equivalent width of a spectral on the stellar parameters. Also, an analysis on the potential use of EW vs $T_{\rm eff}$ plots to identify line contamination was presented. In these regards, the methodology followed to find and identify the contaminators of our preliminary set of lines was also developed so it could be used for another star with different values of stellar parameters. Finally, apart from the three aforementioned objectives of this study, the most relevant result of this work was the development of computational packages in IDL that converted the output from the model atom and synthetic spectra calculation to the input required by the abundance analysis package, so that future studies with different model atoms and model atmospheres be performed quicker.

References

[1] Simón-Díaz, S. *Interaction between massive stars and the interstellar medium in galactic HII regions*, Instituto de astrofísica de Canarias, 2005

[2] García-Rojas et al. *The Cocoon nebula and its ionizing star: do stellar and nebular abundances agree?*, A&A, volume 571, pages A93, 2014

[3] Stasinska G et al, *Oxygen in the universe*, EAS publication series, 2012

[4] David F. Gray, *The observation and analysis of stellar photospheres*, Cambridge university press, 2008

[5] Anil K. Pradhan & Sultana N. Nahar, *Atomic astrophysics and spectroscopy*, Cambridge university press, 2011

[6] Kubát Jirí, *Basics of the NLTE Physics*, GeoPlanet: Earth and Planetary Sciences, Springer International Publishing, pages 149–157, 2014

[7] Przybilla, N., *Non-LTE Model Atom Construction*, EAS Publications Series, volume 43, pages 115-133, 2010

[8] Simón-Díaz S. *A Modern Guide to Quantitative Spectroscopy of Massive OB Stars"*, Reviews in Frontiers of Modern Astrophysics, Springer International Publishing, pages 155-187, 2020

[9] Osorio Y., *maKe Atoms Simple (KAS), a tool to create, manipulate and combine model atoms*, 2018

[10] Hubeny I., *A computer program for calculating non-LTE model stellar atmospheres*, Computer Physics Comm, volume 52, 1988

[11] Van Hoof P.A.M, *Recent Development of the Atomic Line List*, Galaxies, volume 6, 2018

[12] Lanz T. & Hubeny I., *A Grid of NLTE Line-blanketed Model Atmospheres of Early B-Type Stars*, The Astrophysical Journal Supplement Series, volume 169, pages 83-104, 2007

[13] Simón-Díaz S., *The chemical composition of the Orion star forming region*, Astronomy & Astrophysics, 2018

[14] National Institute of Standards and Technology, *About NIST*, https://www.nist.gov/about-nist, 2015

[15] The Opacity project-The Iron project, *TOPbase*, http://cdsweb.u-strasbg.fr/topbase/topbase.html, 2009

[16] Myles W. Jackson, *Spectrum of Belief: Joseph von Fraunhofer and the Craft of Precision Optics*, MIT press, 2000.